

PtdIns(4,5)P₂ stabilizes active states of GPCRs and enhances selectivity of G-protein coupling

Hsin-Yung Yen^{1,2}, Kin Kuan Hoi¹, Idir Liko^{1,2}, George Hedger³, Michael R. Horrell³, Wanling Song³, Di Wu¹, Philipp Heine⁴, Tony Warne⁵, Yang Lee⁵, Byron Carpenter^{5,6}, Andreas Plückthun⁴, Christopher G. Tate⁵, Mark S. P. Sansom^{3*} & Carol V. Robinson^{1*}

G-protein-coupled receptors (GPCRs) are involved in many physiological processes and are therefore key drug targets¹. Although detailed structural information is available for GPCRs, the effects of lipids on the receptors, and on downstream coupling of GPCRs to G proteins are largely unknown. Here we use native mass spectrometry to identify endogenous lipids bound to three class A GPCRs. We observed preferential binding of phosphatidylinositol-4,5-bisphosphate (PtdIns(4,5)P₂) over related lipids and confirm that the intracellular surface of the receptors contain hotspots for PtdIns(4,5)P₂ binding. Endogenous lipids were also observed bound directly to the trimeric G α_i β γ protein complex of the adenosine A_{2A} receptor (A_{2A}R) in the gas phase. Using engineered G α subunits (mini-G α_s , mini-G α_i and mini-G α_{12})², we demonstrate that the complex of mini-G α_s with the β_1 adrenergic receptor (β_1 AR) is stabilized by the binding of two PtdIns(4,5)P₂ molecules. By contrast, PtdIns(4,5)P₂ does not stabilize coupling between β_1 AR and other G α subunits (mini-G α_i or mini-G α_{12}) or a high-affinity nanobody. Other endogenous lipids that bind to these receptors have no effect on coupling, highlighting the specificity of PtdIns(4,5)P₂. Calculations of potential of mean force and increased GTP turnover by the activated neurotensin receptor when coupled to trimeric G α_i β γ complex in the presence of PtdIns(4,5)P₂ provide further evidence for a specific effect of PtdIns(4,5)P₂ on coupling. We identify key residues on cognate G α subunits through which PtdIns(4,5)P₂ forms bridging interactions with basic residues on class A GPCRs. These modulating effects of lipids on receptors suggest consequences for understanding function, G-protein selectivity and drug targeting of class A GPCRs.

The emerging view from biophysical studies of GPCRs is that they exist as ensembles of discrete conformations that can be influenced by ligands, regulatory proteins, pH, ions and, potentially, lipid molecules³. The complex roles of these conformational ensembles in signalling pathways are further compounded by the combinatorial effects of the multiple distinct heterotrimeric complexes formed from 21 G α , 6 G β and 12 G γ subunits. Investigating the relationship between GPCRs, small molecule modulators and numerous binding partners is therefore challenging, owing to the difficulty of observing the complexity of these interactions directly. A previous study characterized interactions of lipids with the β_2 adrenergic receptor (β_2 AR) in high-density lipoparticles⁴ to which phospholipids were added exogenously, but did not address the selectivity and effects of different phosphatidylinositol (PI) phosphate lipids on coupling with downstream effectors. In this study, we develop and apply high-resolution native mass spectrometry to interrogate endogenous lipid-receptor interactions^{5,6} of three class A GPCRs: the β_1 adrenergic receptor (β_1 AR), the adenosine A_{2A} receptor (A_{2A}R), and neurotensin receptor 1 (NTSR1). We reveal effects of PtdIns(4,5)P₂ that stabilize these receptors in active states, increase GTPase activity and enhance selectivity of coupling to G proteins.

First, we considered the endogenous lipids that bind directly to β_1 AR and the stabilized NTSR1 (HTGH4- Δ IC3B)⁷, which were expressed in and purified from insect cells and *Escherichia coli*, respectively. Peaks corresponding to lipid adducts were observed for β_1 AR and for NTSR1 (Fig. 1a and Extended Data Fig. 1a). Collisional dissociation of protein-lipid complexes allowed us to identify two major classes of lipids bound to β_1 AR, the phosphatidylserines (PS) (34:2 and 36:2) and PI phosphates (42:5), as well as phosphatidic acid (PA) (36:2), which bound to NTSR1 (Extended Data Fig. 1b, c and Extended Data Table 1). To investigate this selectivity, we incubated NTSR1 with PA and other anionic lipids (PS and PI), a zwitterionic lipid (phosphatidylcholine (PC)), and a neutral lipid (diacylglycerol (DAG)). Analysis of the resulting native mass spectra show that NTSR1 interacts preferentially with PA, PS and PI (Extended Data Fig. 2a–e). We did not observe apparent binding of phosphatidylglycerol (PG) to NTSR1, although PG has been reported to increase G-protein activation of NTSR1 in a nanodisc⁸. It is possible that PG affects the local net charge at the receptor-lipid interface. Similarly, β_1 AR, when incubated with detergent-solubilised PS (16:0–18:1) or phosphatidylinositol-4-phosphate (PtdIns(4)P) (18:1–18:1), showed higher affinity towards PtdIns(4)P than to PS (Fig. 1a and Extended Data Fig. 2f, g).

To probe the selectivity of different PI derivatives we incubated β_1 AR with equimolar ratios of PI, PtdIns(4)P, phosphatidylinositol-4,5-bisphosphate (PtdIns(4,5)P₂) and phosphatidylinositol-3,4,5-trisphosphate (PtdIns(3,4,5)P₃), all containing the same acyl chains (18:1–18:1). Plotting intensity of peaks corresponding to lipid-bound states in the mass spectrum, relative to those of the apo protein, showed that PtdIns(4,5)P₂ had a higher affinity than PtdIns(4)P for β_1 AR (Fig. 1b). In the case of PtdIns(3,4,5)P₃, which contains one more phosphate group than PtdIns(4,5)P₂, binding to β_1 AR was reduced to a similar level as observed for PI. This demonstrates that binding is selective for the head group of PtdIns(4,5)P₂. We performed similar experiments for NTSR1 and A_{2A}R, and in both cases (PtdIns(4,5)P₂) was found to bind with the highest affinity (Extended Data Fig. 3), implying that all three class A GPCRs contain preferential binding sites for PtdIns(4,5)P₂.

We performed coarse-grained molecular dynamics (CGMD) simulations (Extended Data Fig. 4) to characterize the molecular nature of GPCR-PtdIns(4,5)P₂ interactions in a phospholipid bilayer environment⁹. PtdIns(4,5)P₂ molecules bound at the interface formed by the cytoplasmic loops linking transmembrane helix (TM)1, TM2, TM4 and TM7 of NTSR1; this binding was mediated via interactions between the phosphorylated inositol head group and basic protein side chains (Fig. 1c and Extended Data Fig. 4a). Simulation of NTSR1-PS interactions indicated that these were lower-intensity, diffuse interactions that did not compete with PtdIns(4,5)P₂ (Extended Data Fig. 4c). Similar interactions were seen with β_1 AR, which also exhibited the capacity to interact with PtdIns(4,5)P₂ via the positively charged intracellular surfaces of TM5, TM6 and TM7 (Extended Data Fig. 4b). A more extensive comparison of simulations for nine class A GPCRs (Extended Data

¹Chemical Research Laboratory, University of Oxford, Oxford, UK. ²Omass Technologies, Kidlington, UK. ³Department of Biochemistry, University of Oxford, Oxford, UK. ⁴Biochemisches Institut, Universität Zürich, Zurich, Switzerland. ⁵MRC Laboratory of Molecular Biology, Cambridge, UK. ⁶Present address: Warwick Integrative Synthetic Biology Centre, School of Life Sciences, The University of Warwick, Coventry, UK. *e-mail: mark.sansom@bioch.ox.ac.uk; carol.robinson@chem.ox.ac.uk

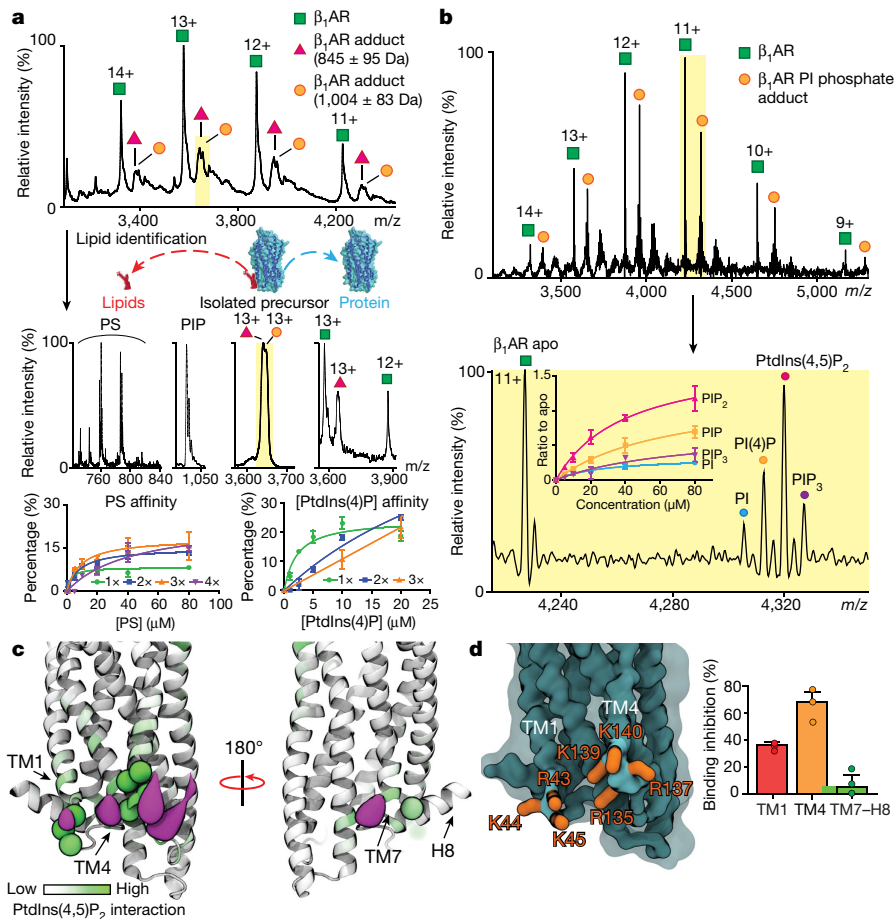


Fig. 1 | Identification of endogenous lipids, preferential binding of PI(4,5)P₂, molecular dynamics simulation and site-directed mutagenesis define intracellular PtdIns(4,5)P₂-binding hotspots.

a, Mass spectrum of β_1 AR (agonist free, green; charge state is shown) and β_1 AR adducts (red, orange). Peaks (highlighted yellow) are selected in the quadrupole and analysed by tandem mass spectrometry. Phosphatidylserine (PS) and PtdIns(4)P (PIP) were identified in the resulting mass spectra. Binding curves plotted against lipid concentration confirm preferential binding of PtdIns(4)P over PS. **b**, Mass spectra of β_1 AR following incubation with an equimolar solution containing PI, PtdIns(4)P, PtdIns(4,5)P₂ and PtdIns(3,4,5)P₃. Binding curves confirm favourable binding of PtdIns(4,5)P₂. **c**, CGMD simulation for

NTSR1(TM86V- Δ IC3B) embedded in a lipid bilayer containing mixed PC and PtdIns(4,5)P₂. Green spheres represent basic residues with high levels of interaction with lipids; purple surfaces represent regions with high density of occupation by PtdIns(4,5)P₂ (0.6-nm distance cut-off based on the radial distribution of coarse-grained particles). **d**, Left, highlighted residues are mutated in NTSR1(TM86V- Δ IC3B): TM1 (R43G, K44G and K45G; red), TM4 (R135I, R137T, K139L and K140L; orange) and TM7-H8 (R311N; green). Right, inhibition of PtdIns(4,5)P₂ binding. Data are mean \pm s.d. from three independent experiments. Results indicate that mutations on the TM4 interface have a greater effect than those on the TM1 and TM7-H8 interfaces. Binding curves in **a** and **b** are plotted as mean \pm s.d. of three replicates from one experiment.

Fig. 4d) showed that this pattern of interactions with PtdIns(4,5)P₂ at the intracellular ends of transmembrane helices is conserved, suggesting that it is structurally and/or functionally significant.

To locate preferential binding sites for PtdIns(4,5)P₂, we performed site-directed mutagenesis on NTSR1, mutating residues that we identified as forming contacts with PtdIns(4,5)P₂ (Fig. 1d) to residues that retain the expression and folded state of the receptor¹⁰. We developed a mass-spectrometry-based strategy to analyse the effect of these mutations on PtdIns(4,5)P₂ binding (Extended Data Fig. 5a). Mutating selected Lys or Arg residues to residues of lower mass decreased the molecular weight of the receptor in comparison to the unmodified parental receptor. When incubated with PtdIns(4,5)P₂, an equimolar solution of mutant and unmodified receptor is presented with an identical lipid environment and can be resolved by mass spectrometry. Attenuation of PtdIns(4,5)P₂ binding was observed in TM1 (35 \pm 0.03%) and TM4 (70 \pm 0.13%) (Fig. 1d and Extended Data Fig. 5b), implying that the cytoplasmic surfaces of these receptors contain hotspots for PtdIns(4,5)P₂ binding.

On the basis of the location of these sites on the cytoplasmic surface, we hypothesized that PtdIns(4,5)P₂ binding influences downstream G-protein coupling. To investigate this, we developed a

mass-spectrometry-based assay in which the pentameric complex of A_{2A}AR (A_{2A}AR-mini-G α_s $\beta\gamma$ -Nb35; Nb35 is a stabilizing nanobody)^{11,12} was preserved in vacuum. The heteropentamer separated into several subcomplexes following collision-induced dissociation, and PS and PI were observed to be directly bound to A_{2A}AR at higher abundance than they were before G-protein coupling (Fig. 2a and Extended Data Fig. 3d). We reasoned that in receptor-G α_s $\beta\gamma$ complexes, these lipids may have a stabilizing role, thereby, in turn, increasing signalling. To investigate these effects, we measured the GTPase activity of G α_s $\beta\gamma$ when coupled to active NTSR1 (bound to neurotensin₈₋₁₃) in the presence or absence of PtdIns(4,5)P₂. We found that GTP hydrolysis was enhanced to 1.3-fold in the presence of PtdIns(4,5)P₂. Therefore, PtdIns(4,5)P₂ enhances both G-protein coupling and GTPase activity (Fig. 2b).

Because of the instability of the trimeric G-protein complex, it is not possible to explore the effects of lipids on coupling in an unbiased way. We therefore investigated receptor complexes formed with engineered mini-G subunits that recapitulate the increase in agonist affinity observed upon coupling with the native heterotrimeric G protein (Fig. 2c). We recorded mass spectra of thermostabilized β_1 AR in complex with mini-G_s. We found increased association of lipids when

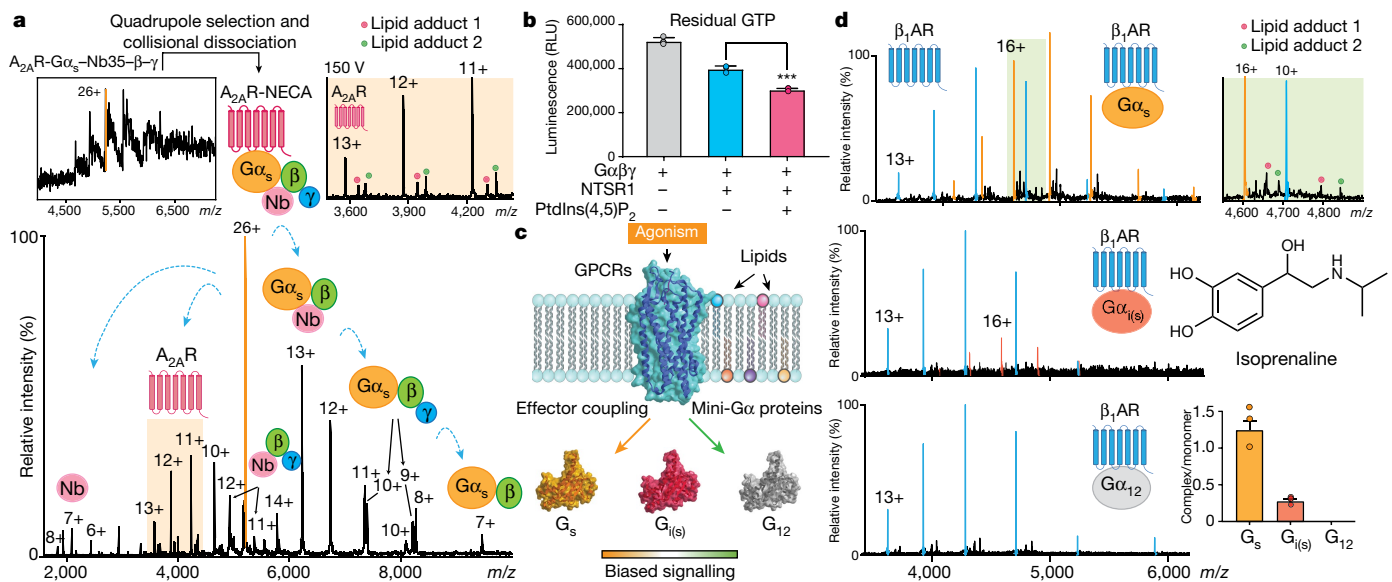


Fig. 2 | Selectivity of G-protein coupling and the presence of endogenous lipids on coupled receptors. **a**, A representative mass spectrum of $A_{2A}R$ receptor coupled to a trimeric G-protein complex in complex with the stabilizing nanobody Nb35 (top left) from three independent experiments. Isolating and subjecting charge state 26+ (orange peak) to collision-induced dissociation results in dissociation into subcomplexes (bottom) and the receptor with lipid adducts (top right). **b**, GTPase assays indicate an increase of GTP hydrolysis by active NTSR1 coupled to trimeric $G\alpha_i\beta\gamma$ in the presence of PtdIns(4,5)P₂. *** $P < 0.001$;

Student's t -test comparing the effect of PtdIns(4,5)P₂ (one variable) on receptor-induced GTPase activation. Bars show mean \pm s.d., points show data from three independent experiments. **c**, Schematic representation of the influence of lipids and agonists on the binding of mini-G proteins. **d**, Mass spectra of isoprenaline-bound β_1AR with three different mini-G subunits (mini-G_s, mini-G_{i(s)} and mini-G₁₂). Enhanced coupling and lipid adducts are observed in the presence of G_s (top right). In bottom right, bars show mean \pm s.d., points show data from three independent experiments.

β_1AR was in a complex with mini-G_s (Fig. 2d). The stability of the receptor–mini-G_s complex allowed us to investigate the selectivity towards different subtypes of G α subunits (G_s, G $\alpha_{i/o}$ and G $\alpha_{12/13}$). We investigated the coupling of agonist-bound β_1AR to mini-G_{i(s)}, which was engineered from mini-G_s by introducing nine mutations on the α_5 helix to the corresponding residues on G α_i . We performed a similar experiment with the analogous mutant of G α_{12} , in which we transferred the mutations from mini-G_s to G₁₂². In comparison to mini-G_s, there was a reduced degree of coupling with mini-G_{i(s)} and virtually no coupling with mini-G₁₂ (Fig. 2d).

To investigate the effect of PtdIns(4,5)P₂ on GPCR–mini-G_s interactions, we incubated agonist-bound β_1AR with mini-G_s in the presence of lipid and compared the mass spectrometry peaks corresponding to the lipid-bound protein. Although the complex can form in the absence of lipids, or with only one bound PtdIns(4,5)P₂, complex formation is markedly enhanced (2.7- or 4.5-fold compared to the receptor without lipid, respectively) in the presence of two or three PtdIns(4,5)P₂ molecules (Fig. 3a, g). We observed a similar effect in a time-course experiment in which coupling of mini-G_s to β_1AR increased by $21 \pm 6\%$ when two PtdIns(4,5)P₂ molecules were bound and by a further $12 \pm 5\%$ when three PtdIns(4,5)P₂ molecules were bound (Extended Data Fig. 6a).

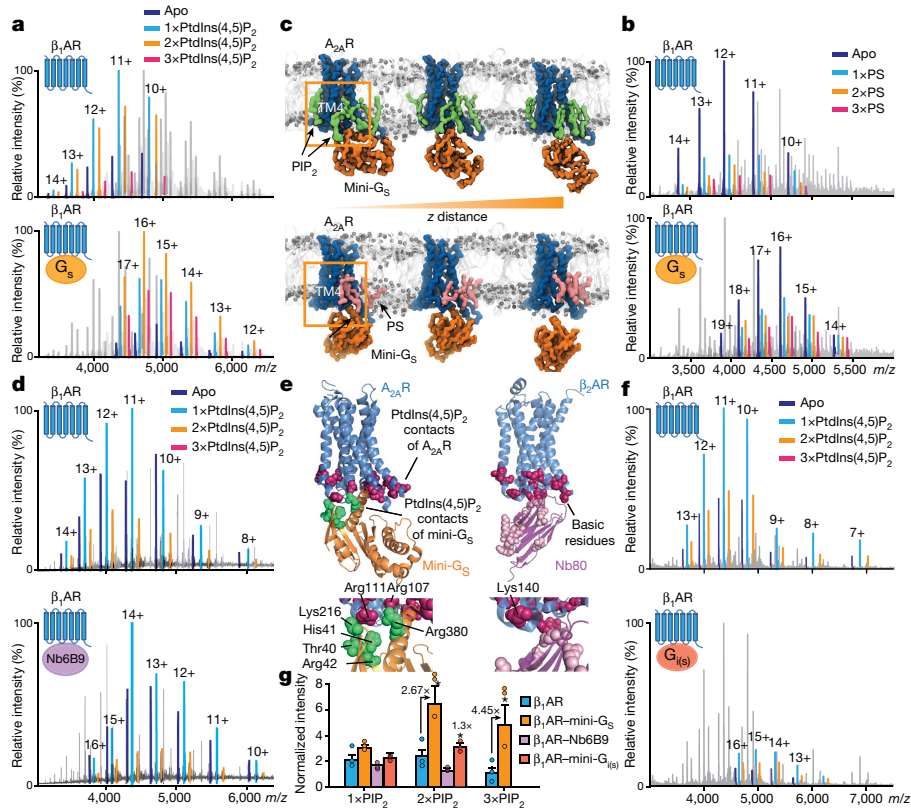
We examined the effect of PS, an anionic lipid that was endogenously bound to β_1AR (Fig. 1a), on coupling of mini-G_s. We performed analogous experiments using a threefold higher concentration of PS than that used in the experiments with PtdIns(4,5)P₂ to reflect the reduced affinity of β_1AR for PS (Fig. 3b and Extended Data Fig. 2). Mass spectra showed only a slight increase in the extent of mini-G_s coupling as a function of PS binding. This reduced effect in comparison to PtdIns(4,5)P₂ suggests that the electrostatic interactions of the polyanionic lipid headgroups in PtdIns(4,5)P₂, which have multiple basic sidechains, are necessary for receptor coupling (as observed for Kir channels, for example¹³), and that such interactions do not occur with PS.

These data indicate that additional PtdIns(4,5)P₂, but not PS, stabilize the complex once receptor coupling has occurred. Therefore, we used

potential of mean force (PMF) calculations¹⁴ to explore the effect of PtdIns(4,5)P₂ binding on the free-energy landscape of $A_{2A}R$ –mini-G_s interactions¹⁵. Comparison of PMFs for PtdIns(4,5)P₂-bound versus PS-bound receptor in a lipid bilayer indicates that the interaction of mini-G_s with $A_{2A}R$ is stabilized significantly (50 ± 10 kJ mol⁻¹) in the presence of PtdIns(4,5)P₂ compared with PS (Fig. 3c and Extended Data Fig. 6b). The presence of PtdIns(4,5)P₂ at the interface between the receptor and mini-G_s in the PMF calculation implies that PtdIns(4,5)P₂ molecules form bridging interactions to stabilize the complex.

The increase in PtdIns(4,5)P₂ binding to β_1AR when it is coupled to mini-G_s could be a result of either (i) active conformations of receptors binding more PtdIns(4,5)P₂ than their inactive counterparts, or (ii) positively charged residues in mini-G_s, at the receptor–G protein interface, recruiting additional PtdIns(4,5)P₂ molecules following coupling. To investigate the dependence of PtdIns(4,5)P₂ binding on receptor conformation, we incubated PtdIns(4,5)P₂ with β_1AR (co-purified with the agonist isoprenaline) containing an E130W mutation to stabilize ligand-free β_1AR without affecting G-protein coupling¹⁶. We observed a $31 \pm 1\%$ increase in PtdIns(4,5)P₂ binding to the β_1AR –isoprenaline complex versus ligand-free β_1AR (Extended Data Fig. 6c). Whereas in general, transition to active states is thought to involve substantial movements of TM5 and TM6, intracellular loop (ICL)2 was also found to undergo significant changes during activation of the κ -opioid receptor¹⁷. These results are consistent with PtdIns(4,5)P₂ stabilizing active states of receptors via binding hotspots directly on ICL2, and, more generally, via diffuse intracellular PtdIns(4,5)P₂-binding sites.

To explore the second possibility, in which additional PtdIns(4,5)P₂-binding sites form following coupling, we carried out CGMD simulations for $A_{2A}R$ –mini-G_s, which is, to our knowledge, the only available structure of a receptor–mini-G complex. In addition to the contacts described above, PtdIns(4,5)P₂ interacted with residues of mini-G_s proximal to the lipid contacts in TM3, TM4 and TM5 of $A_{2A}R$ (Fig. 3e). To investigate the significance of these additional binding sites we used a nanobody (Nb6B9)¹⁸, in which the lipid-binding residues identified in mini-G_s are absent¹² (Extended Data Fig. 7). Structures of receptors bound to Nb6B9 or to mini-G_s are virtually identical¹⁹



of β_1 AR and β_1 AR–mini-G_s ($n = 3$ independent experiments) in the presence of PtdIns(4,5)P₂ and the agonist isoprenaline. Coloured peaks highlight β_1 AR lipid-bound states (top) and β_1 AR–mini-G_s lipid-bound states (bottom). **b**, Representative mass spectra of β_1 AR and β_1 AR–mini-G_s ($n = 3$ independent experiments) in the presence of PS and the agonist isoprenaline. There is no marked difference in PS binding between β_1 AR and β_1 AR–mini-G_s. **c**, Snapshots of steered molecular dynamics simulations to separate mini-G_s and A_{2A}R in the presence of PtdIns(4,5)P₂ (green) and PS (pink). Orange outlines highlight the different binding modes of PtdIns(4,5)P₂ and PS to the receptor. The interaction of mini-G_s with A_{2A}R is stabilized by ~ 50 kJ mol⁻¹ in the presence of PtdIns(4,5)P₂ relative to PS (Extended Data Fig. 6b). **d**, Representative mass spectra

(root mean square displacement (r.m.s.d.) = 0.4–0.6 Å). Comparing PtdIns(4,5)P₂ binding to the receptor and to the receptor–nanobody complex, we found that the degree of PtdIns(4,5)P₂ binding was very similar (Fig. 3d, g). The absence of lipid-binding residues in Nb6B9 (Fig. 3e) explains the insensitivity of the receptor–nanobody complex to PtdIns(4,5)P₂ and implies that PtdIns(4,5)P₂ molecules enhance coupling via interactions that are specific to the receptor and mini-G_s. Lipids such as PS, in which the polyanionic headgroups are absent, would not be able to induce this effect.

To investigate the possibility that residues specific to mini-G_s, that are not present in other G proteins, mediate bridging, we investigated the effects of PtdIns(4,5)P₂ on the coupling of mini-G_{i(s)} to agonist-bound β_1 AR. We found that coupling was increased in the presence of PtdIns(4,5)P₂, but to a lesser extent than with mini-G_s (Fig. 3f, g). Given the established role in coupling to receptors of TM5 in G α_s (R380), together with residues identified by molecular dynamics simulation (Fig. 3e), and the fact that these residues are substituted in G α_i (E40, V41, K42, D216 and T380), differences in PtdIns(4,5)P₂ binding can be attributed to disruption of these PtdIns(4,5)P₂-bridging sites. It therefore follows that PtdIns(4,5)P₂-binding sites on G α_s , which are not present on G α_i , enable simultaneous binding of the β_1 AR to the G protein to which it has highest affinity. Consequently, we propose that PtdIns(4,5)P₂ acts as an allosteric modulator, binding to the

intracellular side of the receptor, stabilizing the active state and enhancing selectivity of G-protein coupling. This coupling is then further stabilized by PtdIns(4,5)P₂ molecules bridging between the receptor and the G protein.

More generally, it has been established that the cytoplasmic face of GPCRs undergoes conserved conformational changes to allow coupling of G proteins²⁰; the cytoplasmic ends of TM5 and TM6 move outwards, and TM7 moves slightly inwards. Synthetic molecules that bind at the TM5–TM6–TM7 cytoplasmic interface act as negative allosteric modulators that inhibit the activation of GPCRs by preventing their movement and consequently reducing the affinity of agonists at the orthosteric binding pocket^{21,22}. Here we highlight another role of the cytoplasmic interface, which recruits PtdIns(4,5)P₂, thereby stabilizing the active G-protein-bound state of the receptor. Simultaneous binding of the PtdIns(4,5)P₂ head group to both the G α subunit and conserved TM4 residues on a number of class A receptors that are not present on class B receptors suggests the generality of this mechanism for selectively stabilizing active states of class A GPCRs (Extended Data Figs. 4d, 8).

As the local concentration of PtdIns(4,5)P₂ in the membrane has the potential to be modulated by different signalling pathways, such as receptor tyrosine kinases or Ca²⁺ signalling, crosstalk with GPCRs through PtdIns(4,5)P₂ may represent an additional mode of regulation

in the cell²³. Further, the potential to stabilize the active conformation of G-protein-coupled receptors through the binding of potent small molecules that mimic the bridging effects of the PtdIns(4,5)P₂ head group provides a further avenue for stabilizing active states of GPCRs for therapeutic purposes. As PtdIns(4,5)P₂ is able to discriminate between different G-protein subunits, and is likely to also influence binding to β -arrestin, there are potential benefits in developing novel compounds that bind specifically to different G-protein-coupled or β -arrestin-bound states, thereby providing a new perspective for rational design of novel biased allosteric agonists.

Online content

Any Methods, including any statements of data availability and Nature Research reporting summaries, along with any additional references and Source Data files, are available in the online version of the paper at <https://doi.org/10.1038/s41586-018-0325-6>.

Received: 24 July 2017; Accepted: 14 May 2018;

Published online 11 July 2018.

- Hauser, A. S., Attwood, M. M., Rask-Andersen, M., Schiöth, H. B. & Gloriam, D. E. Trends in GPCR drug discovery: new agents, targets and indications. *Nat. Rev. Drug Discov.* **16**, 829–842 (2017).
- Nehmé, R. et al. Mini-G proteins: Novel tools for studying GPCRs in their active conformation. *PLoS One* **12**, e0175642 (2017).
- Zocher, M., Zhang, C., Rasmussen, S. G., Kobilka, B. K. & Muller, D. J. Cholesterol increases kinetic, energetic, and mechanical stability of the human β_2 -adrenergic receptor. *Proc. Natl Acad. Sci. USA* **109**, E3463–E3472 (2012).
- Dawaliby, R. et al. Allosteric regulation of G protein-coupled receptor activity by phospholipids. *Nat. Chem. Biol.* **12**, 35–39 (2016).
- Gault, J. et al. High-resolution mass spectrometry of small molecules bound to membrane proteins. *Nat. Methods* **13**, 333–336 (2016).
- Yen, H. Y. et al. Ligand binding to a G protein-coupled receptor captured in a mass spectrometer. *Sci. Adv.* **3**, e1701016 (2017).
- Egloff, P. et al. Structure of signaling-competent neurotensin receptor 1 obtained by directed evolution in *Escherichia coli*. *Proc. Natl Acad. Sci. USA* **111**, E655–E662 (2014).
- Inagaki, S., Ghirlando, R. & Grishammer, R. Biophysical characterization of membrane proteins in nanodiscs. *Methods* **59**, 287–300 (2013).
- Hedger, G. & Sansom, M. S. P. Lipid interaction sites on channels, transporters and receptors: Recent insights from molecular dynamics simulations. *BBA-Biomembranes* **1858**, 2390–2400, (2016).
- Schlinkmann, K. M. et al. Critical features for biosynthesis, stability, and functionality of a G protein-coupled receptor uncovered by all-versus-all mutations. *Proc. Natl Acad. Sci. USA* **109**, 9810–9815 (2012).
- Carpenter, B., Nehmé, R., Warne, T., Leslie, A. G. W. & Tate, C. G. Structure of the adenosine A_{2A} receptor bound to an engineered G protein. *Nature* **536**, 104–107 (2016).
- Rasmussen, S. G. et al. Structure of a nanobody-stabilized active state of the β_2 adrenoceptor. *Nature* **469**, 175–180 (2011).
- Hansen, S. B., Tao, X. & MacKinnon, R. Structural basis of PIP₂ activation of the classical inward rectifier K⁺ channel Kir2.2. *Nature* **477**, 495–498 (2011).
- Roux, B. The calculation of the potential of mean force using computer simulations. *Comput. Phys. Commun.* **91**, 275–282 (1995).
- Domański, J., Hedger, G., Best, R. B., Stansfeld, P. J. & Sansom, M. S. P. Convergence and sampling in determining free energy landscapes for membrane protein association. *J. Phys. Chem. B* **121**, 3364–3375 (2017).
- Roth, C. B., Hanson, M. A. & Stevens, R. C. Stabilization of the human β_2 -adrenergic receptor TM4–TM3–TM5 helix interface by mutagenesis of Glu122³⁴¹, a critical residue in GPCR structure. *J. Mol. Biol.* **376**, 1305–1319 (2008).
- Che, T. et al. Structure of the nanobody-stabilized active state of the kappa opioid receptor. *Cell* **172**, 55–67 e15, (2018).
- Miller-Gallacher, J. L. et al. The 2.1 Å resolution structure of cyanopindolol-bound β_1 -adrenoceptor identifies an intramembrane Na⁺ ion that stabilises the ligand-free receptor. *PLoS One* **9**, e92727 (2014).
- Injin, B. & Hee-Jung, C. Structural features of β_2 adrenergic receptor: crystal structures and beyond. *Mol. Cells* **38**, 105–111 (2015).
- Venkatakrishnan, A. J. et al. Diverse activation pathways in class A GPCRs converge near the G-protein-coupling region. *Nature* **536**, 484–487 (2016).
- Zheng, Y. et al. Structure of CC chemokine receptor 2 with orthosteric and allosteric antagonists. *Nature* **540**, 458–461 (2016).
- Liu, X. et al. Mechanism of intracellular allosteric β_2 AR antagonist revealed by X-ray crystal structure. *Nature* **548**, 480–484 (2017).
- Gavi, S., Shumay, E., Wang, H. Y. & Malbon, C. C. G-protein-coupled receptors and tyrosine kinases: crossroads in cell signaling and regulation. *Trends Endocrinol. Metab.* **17**, 48–54 (2006).

Acknowledgements C.V.R. acknowledges an ERC Advanced Grant ENABLE (641317), an MRC Programme Grant (G1000819) and a Wellcome Trust Investigator Award (104633/Z/14/Z). Further support was provided by the MRC (G.H.), the Royal Society Newton International Fellowship (W.S.), and the BBSRC (M.S.P.S.; BB/L002558/1) and the Wellcome Trust (M.S.P.S.; 092970/Z/10/Z). This work used the ARCHER UK National Supercomputing Service (<http://www.archer.ac.uk>), supported by EPSRC. A.P. was funded by the Schweizerischer Nationalfonds Grant (31003A_153143). C.G.T. acknowledges the MRC (MC_U105197215), an ERC Advanced Grant EMPSI (339995) and funding from Heptares Therapeutics. We thank M. Hillenbrand for providing Sf9 cells.

Reviewer information *Nature* thanks A. Lee, C. Reynolds, J. Whitelegge and the other anonymous reviewer(s) for their contribution to the peer review of this work.

Author contributions H.-Y.Y., K.K.H. and I.L. performed all mass spectrometry experiments on the GPCR, mini-G_s and nanobody. D.W. performed lipidomics. G.H., M.R.H., W.S., and M.S.P.S. performed molecular dynamics simulations and analyses. P.H. purified the NTSR1 receptor in the apo state. T.W. purified β_1 AR, Y.L. purified A_{2A}R and B.C. purified mini-G_s. A.P., C.G.T., M.S.P.S. and C.V.R. supervised the research and H.-Y.Y. and C.V.R. wrote the paper with contributions from all authors.

Competing interests H.-Y.Y. and I.L. are founders and employees of OMass Technologies. C.V.R. is a founder of and consultant for OMass Technologies.

Additional information

Extended data is available for this paper at <https://doi.org/10.1038/s41586-018-0325-6>.

Supplementary information is available for this paper at <https://doi.org/10.1038/s41586-018-0325-6>.

Reprints and permissions information is available at <http://www.nature.com/reprints>.

Correspondence and requests for materials should be addressed to M.S.P.S. or C.V.R.

Publisher's note: Springer Nature remains neutral with regard to jurisdictional claims in published maps and institutional affiliations.

METHODS

Constructs and proteins. We used expression plasmids for two stabilized variants of rat NTSR1^{7,24}. NTSR1 (HTGH4- Δ IC3B) contains the protein sequence from amino acids 50 to 390 with deletion of ICL3 (residues 273–290) and 26 thermostabilizing point mutations. It should be noted that this construct is only 80% identical to the wild-type. NTSR1 (HTGH4 43–421) contains the intact protein sequence from residues 43 to 421, with the same stabilizing mutations as NTSR1 (HTGH4- Δ IC3B). Purified thermostabilized turkey (*Meleagris gallopavo*) β_1 AR, human wild-type A_{2A} AR, engineered G_{α_s} (mini- G_s) and nanobody Nb6B9 were used for mass spectrometry analysis^{11,25,26}. The following point mutations on β_1 AR were used throughout: R68S, M90V, F327A, F338M (thermostabilizing); C116L (to increase protein expression); R284K (residue equivalent to β_2 AR designed to improve Nb80 binding); C358A (prevention of potential palmitoylation). In order to purify receptor in the unliganded state, a construct with the same thermostabilizing mutations but slightly different lengths of TM1 was introduced with an additional mutation (E130W) to stabilize the receptor. The use of an N-terminal TrxA fusion (C32S and C35S) on the receptor was necessary to confirm formation of a complex on SDS gels. Insect cell lines for receptor overexpression (Sf9 and Tni) were obtained from Invitrogen and Sf9 cells for heterotrimeric G protein production were provided by M. Hillenbrand. All cells were confirmed to be free from mycoplasma contamination.

Protein expression and purification. *Expression and purification of β_1 AR.* *M. gallopavo* β_1 AR constructs (β 118 and β 114-E130W) were based on the previously published thermostabilized β_1 AR44-m23 construct²⁷ but contained only four (R68S, M90V, F327A, F338M) of the original six thermostabilizing mutations, as the two mutations on TM5 and TM6 (Y227A and A282L) were not included. The omission of these two mutations resulted in constructs that demonstrated coupling to G proteins and to G protein mimetic nanobody Nb80 along with high affinity agonist binding²⁵. The constructs included *E. coli* Thioredoxin fused to the N terminus of TM1 and the mutations C116L to improve expression and C358A to prevent potential palmitoylation. Both constructs were expressed in Sf9 insect cells using recombinant baculoviruses prepared using the transfer vector pAcGP67B (BD Biosciences) and BacPAK6 linearized baculovirus DNA (Oxford Expression Technologies). The membrane containing the expressed receptor was solubilized and purified in 2% and 0.02% dodecylmaltoside (DDM, Generson), respectively, as described previously^{27–29}. For β 118, the final purification step was competitive elution from an alprenolol sepharose ligand-affinity column in 20mM Tris-HCl, pH7.4, 350 mM NaCl and 0.02% DDM supplemented with 1mM isoprenaline, so that the receptor was prepared with bound agonist ligand. The purified receptor was finally concentrated to 15 mg/ml in the alprenolol sepharose elution buffer.

β 114(E130W) contained the mutation E130W, which increased functional expression of β_1 AR¹⁶. This mutation facilitated the preparation of highly purified active receptor without any bound ligand, as the use of a ligand-affinity chromatography step was not necessary to separate non-functional receptor. For β 114(E130W), purification was performed in 0.02% DDM by Ni^{2+} affinity chromatography followed by a thrombin (Sigma) protease cleavage step to remove the His tag before further purification by size-exclusion chromatography (SEC) on a Superdex Increase 200 10/300GL column (GE Healthcare) in 20mM Tris-HCl, pH7.4, 100 mM NaCl and 0.02% DDM, with final concentration to 45 mg/ml.

Expression and purification of A_{2A} AR. The human A_{2A} AR construct (residues 1–308) was modified with a C-terminal histidine tag (His10) preceded by a TEV protease cleavage site, and by the mutation N154A to prevent N-linked glycosylation. The A_{2A} AR was expressed in Tni insect cells using the baculovirus system. Cell membranes were prepared and solubilised with 2% lauryl maltose neopentyl glycol (LMNG, Anatrace) and the receptor was purified by Ni^{2+} affinity chromatography and SEC, using a Superdex Increase 200 10/300GL column (GE) run in 20 mM HEPES pH 7.5, 100 mM NaCl, 10% (v/v) glycerol, 0.01% (w/v) LMNG and concentrated to 10 mg/ml. Purification was as described previously¹¹, with the exception that the receptor was purified without addition of ligand.

Expression and purification of mini- G_s , mini- G_i and mini- G_{12} . The engineered minimal G proteins, mini- G_s construct R414²⁵, mini- G_i construct and mini- G_{12} construct 8² were expressed in *E. coli* and purified by Ni^{2+} affinity chromatography, followed by cleavage of the histidine tag using TEV protease and negative purification on Ni^{2+} -NTA to remove TEV and undigested mini-G protein, and finally SEC to remove aggregated protein as described elsewhere^{25,30}, with final concentration up to 100 mg/ml in 10 mM HEPES, pH 7.5, 100 mM NaCl, 10% v/v glycerol, 1 mM $MgCl_2$, 1 μ M GDP and 0.1 mM TCEP.

Expression and purification of nanobody Nb6B9. A synthetic gene (Integrated DNA Technologies) for Nb6B9^{12,31} was cloned into the plasmid pET-26b(+) (Novagen) with a N-terminal His₆ tag followed by a thrombin protease cleavage site. Expression was in *E. coli* strain BL21 (DE3)RIL (Agilent Technologies) and purification from the periplasmic fraction was by Ni^{2+} affinity chromatography, but with the use of a thrombin (Sigma) protease cleavage step to remove the His tag before concentration to 40 mg/ml.

Preparation of receptor–G-protein complexes. Several receptor–G-protein complexes were prepared for mass spectrometry analysis. A_{2A} AR–mini- $G_{\beta\gamma}$ was prepared by incubating and co-purifying A_{2A} AR, containing a TrxA fusion at the N-terminal, with N-ethyl-carboxamidoadenosine (NECA). The complex with trimeric G proteins complex consisted of mini- G_s , G_{β} , G_{γ} and nanobody Nb35 with receptor:G proteins:Nb35 at a 1:2:4 molar ratio to stabilize the complex. The complex was further purified by gel-filtration chromatography after overnight incubation. β_1 AR–miniG was prepared by incubating β_1 AR co-purified with isoprenaline and the different mini-G proteins (mini- G_s , mini- $G_{i(s)}$ and mini- G_{12}) at 1:1.2 molar ratio. The incubation time was varied to capture the equilibrium of complex formation.

Purification of heterotrimeric G protein. Baculovirus encoding the desired subunits ($\alpha_{11}\beta_1\gamma_1$) was used to express the heterotrimeric G protein in Sf9 cells as previously described³². Cells from a 1-l expression culture were resuspended and lysed in lysis buffer (10 mM HEPES pH 7, 20 mM KCl, 10 mM $MgCl_2$, 10 μ M GDP, 2 mM β -mercaptoethanol, and cComplete protease inhibitor (Roche)). The membranes were pelleted by ultracentrifugation at 108,000g for 35 min and solubilized in solubilisation buffer (50 mM HEPES pH 7, 150 mM NaCl, 10 mM $MgCl_2$, 10 μ M GDP, 2 mM β -mercaptoethanol, 1% decyl- β -D-maltopyranoside (DM) (w/v), 10% (v/v) glycerol, and cComplete protease inhibitor (Roche)) for 3 h. The supernatant was collected after centrifugation at 108,000g for 35 min and incubated with 1.2 ml TALON beads (GE Healthcare) overnight. The beads were collected and washed with ten column volumes wash buffer (30 mM HEPES pH 7, 300 mM NaCl, 10 mM $MgCl_2$, 25 mM imidazole pH 8, 10 μ M GDP, 2 mM β -mercaptoethanol, 10% (v/v) glycerol, and 0.5% (w/v) DM), followed by another twenty column-volume wash of wash buffer containing 40 mM imidazole (pH 8.0), and were eluted with five column volumes elution buffer (30 mM HEPES pH 7, 150 mM NaCl, 1 mM $MgCl_2$, 300 mM imidazole pH 8, 10 μ M GDP, 2 mM β -mercaptoethanol, 10% (v/v) glycerol, and 0.5% (w/v) DM). The protein was further purified by a Superdex 200 Increase PC 3.2/300 column (GE Healthcare) and the protein tag was removed by incubation with human rhinovirus 3C protease (produced in house) overnight. Following buffer exchange to storage buffer (20 mM HEPES pH 7, 100 mM NaCl, 0.1 mM $MgCl_2$, 4 mM β -mercaptoethanol, 10% (v/v) glycerol, and 0.5% (w/v) DM) and reverse immobilized metal affinity chromatography (IMAC) by Ni-NTA superflow beads (GE Healthcare), G-protein complex was concentrated to at least 2 mg/ml for experimental use.

NTSR1 expression. BL21 *E. coli* cells were transformed with the expression plasmid encoding NTSR1 (HTGH4- Δ IC3B) and grown overnight at 37 °C in 20 ml 2YT medium supplemented with 1% (w/v) glucose and 100 μ g/ml ampicillin. Two flasks, each containing each 1 l 2YT medium, 0.5% (w/v) glucose, and 100 μ g/ml ampicillin were inoculated with 10 ml pre-culture and grown to an $A_{600\text{ nm}}$ of 0.5 with shaking at 37 °C. Receptor expression was induced with 1 mM isopropyl- β -D-thiogalactopyranoside (IPTG) and cells were cultivated at 28 °C overnight. Cells were harvested after overnight expression and *E. coli* cell pellets were resuspended in 100 ml solubilisation buffer, containing 100 mM HEPES pH 8.0, 20% (v/v) glycerol and 400 mM NaCl. Resuspended cells were frozen in liquid nitrogen and stored at –80 °C.

Apo NTSR1 purification. The cell pellet was thawed at room temperature. All following steps were carried out at 4 °C. $MgCl_2$ (5 mM), 2 mg DNase I, 200 mg lysozyme, and 20 ml detergent mixture (0.2% (w/v) cholesteryl hemisuccinate Tris salt (CHS) and 2% (w/v) dodecyl- β -D-maltopyranoside (DDM)) were added to the thawed cell pellet. The mixture was incubated for 1 h, followed by cell lysis via mild sonication for 30 min in an ice-water bath. After cell lysis, 0.4 ml 5 M imidazole was added and the mixture was incubated for another 30 min. The suspension was centrifuged for 30 min at 28,000g. The supernatant was mixed with 5 ml TALON resin (Clontech), which had been pre-equilibrated with IMAC binding buffer (25 mM HEPES pH 8.0, 10% (v/v) glycerol, 600 mM NaCl, 0.1% (w/v) DDM and 20 mM imidazole) and incubated overnight on a rolling device. The mixture was loaded into a PD10 column (GE Healthcare) and was washed with 50 ml IMAC binding buffer. Elution of bound protein was performed with 15 ml IMAC elution buffer containing 25 mM HEPES pH 8.0, 10% (v/v) glycerol, 150 mM NaCl, 0.1% (w/v) DDM and 250 mM imidazole. Eluted receptor was concentrated in an Amicon-15 Ultra concentrator with a 100 kDa cut-off (Millipore) to a final volume of less than 2.5 ml. Concentrated receptor sample was loaded on a Sephadex G-25 desalting column (GE Healthcare), pre-equilibrated with 25 mM HEPES pH 8.0, 10% (v/v) glycerol, 150 mM NaCl, 0.1% (w/v) DDM to remove remaining imidazole. Desalted receptor was incubated with 300 μ l 1.6 mg/ml HRV 3C protease for 1 h at 4 °C, followed by addition of 150 μ l 10% (w/v) LMNG and incubation for 1 h at 4 °C. The cleaved protein was diluted threefold with reverse IMAC buffer (10 mM HEPES pH 8.0, 10% (v/v) glycerol, 150 mM NaCl, and 0.01% (w/v) LMNG) and was loaded onto a PD10 column containing 5 ml Ni-NTA beads pre-equilibrated with reverse IMAC buffer. The flow through was collected in an Amicon-15 Ultra concentrator with a 50-kDa cut-off and the resin was further washed with 10 ml buffer. Receptor was concentrated to a final volume of less than 1 ml and was subjected to preparative

SEC using a Superdex 200 10/300 GL column (GE Healthcare), which had been pre-equilibrated with 10 mM HEPES pH 8, 150 mM NaCl, and 0.01% (w/v) LMNG. Peak fractions corresponding to NTSR1(HTGH4- Δ IC3B) were pooled (final volume 3–4 ml) and concentrated in an Amicon-4 Ultra-concentrator with a 50-kDa cut-off to a final protein concentration of approximately 50 μ M. Purified and concentrated NTSR1-H4 was mixed with 10 mM HEPES pH 8, 150 mM NaCl, 0.01% (w/v) LMNG, and 50% (v/v) glycerol to yield a final glycerol concentration of 25%. Aliquots were frozen in liquid nitrogen and stored at -80°C for later use.

Preparation of phospholipids and titration experiment. Phospholipids were purchased from Avanti (Avanti Polar Lipids) and prepared as 3 mM stock solutions in 200 mM ammonium acetate buffer pH 7.5 containing the detergent-mixed micelle preparation, containing DDM and foscholine as previously described³⁵. Phosphate analysis was performed to determine the concentration of phospholipids in solution³⁴. For the titration experiment, 5 μ M buffer-exchanged receptors in 200 mM ammonium acetate buffer pH 7.5 containing the detergent mixtures (DDM, LMNG, and foscholine for NTSR1; DDM and foscholine for β_1 AR and A_{2A}R) were mixed with lipids at various concentration points followed by equilibration at 4 $^{\circ}\text{C}$ for 5 min, by which time lipid binding had stabilized according to our time course measurements. Following mass spectrometry analysis, UniDec (Universal Deconvolution) software was used to quantify the relative abundance of each lipid-bound state³⁵, and statistical analysis was performed using GraphPad Prism, assuming a one-site total binding model.

Lipidomics analysis. Co-purified lipids from recombinant GPCRs were extracted by chloroform-methanol (2:1, v/v) and lyophilized and re-dissolved in 60% acetonitrile (ACN). For LC-MS/MS analysis, the extracted lipids were separated on a C18 column (Acclaim PepMap 100, C18, 75 mm \times 15 μm ; Thermo Scientific) using a Dionex UltiMate 3000 RSLC nano LC System. The buffers and gradient are adapted from a previous protocol³⁶. In brief, the lipids were separated using a binary buffer system at 40 $^{\circ}\text{C}$ using a gradient of 32–99% buffer B at a flow rate of 300 nl/min over 30 min. (Buffer A: (acetonitrile: H₂O (60:40), 10 mM ammonium formate, 0.1% formic acid) and buffer B (propan-2-ol:acetonitrile (90:10), 10 mM ammonium formate, 0.1% formic acid)). The column eluent was delivered via a dynamic nanospray source to a hybrid LTQ Orbitrap mass spectrometer (Thermo Scientific). Typical mass spectrometry conditions were: spray voltage (1.8 kV) and capillary temperature (175 $^{\circ}\text{C}$). The LTQ-Orbitrap XL was operated in negative ion mode using data-dependent acquisition with one MS scan followed by five MS/MS scans³⁷. Survey full-scan mass spectra were acquired in the orbitrap (m/z 350–2,000) with a resolution of 60,000. CID fragmentation in the linear ion trap was performed for the five most intense ions at an automatic gain control target of 30,000 and a normalized collision energy of 38% at an activation of $q = 0.25$ and an activation time of 30 ms.

GTPase assay. The GTPase activity of trimeric G $\alpha_i\beta\gamma$ was measured with the GTPase-Glo assay (Promega). The assay was performed in white 384-well plates (Corning) using purified trimeric G proteins diluted into a GTPase buffer (10 mM HEPES pH 7, 50 mM NaCl, 0.05 mM MgCl₂, 2 mM β -mercaptoethanol, 1 mM DTT, 5% (v/v) glycerol, and 0.25% (w/v) DM) at a final concentration 2.5 μ M in the presence of 5 μ M GTP. The luminescent signal was measured after incubation at room temperature (1 h) following the manufacturer's protocol to indicate the level of residual GTP. To analyse the impact of PtdIns(4,5)P₂ we used NTSR1(HTGH4- Δ IC3B) co-purified with recombinant neurotensin_{8–13} following the method described previously³⁸. The receptor was pre-incubated with detergent-solubilised PtdIns(4,5)P₂ at 1:3 molar ratio (receptor:lipid) in the protein buffer (10 mM HEPES pH 8, 150 mM NaCl, 0.01% (w/v) LMNG) containing 100 nM neurotensin_{8–13} for 15 min on ice. The activated receptor was then added to the reaction mixture containing trimeric G proteins under the condition described above.

Native mass spectrometry of GPCRs. Purified GPCRs were buffer exchanged into 200 mM ammonium acetate buffer pH 7.5 containing the mixed micelle preparation optimized for GPCR analysis as described previously⁶. The concentration of DDM, foscholine and CHS required to form a mixed micelle range from 0.006–0.02%, 0–0.002%, and 0.001–0.01%, respectively, and are optimized for each receptor preparation. The samples were immediately introduced into a modified Q-Exactive mass spectrometer (Thermo), as described previously⁵. Ions were transferred into the higher-energy collisional dissociation (HCD) cell following a gentle voltage gradient (injection flatapole, inter-flatapole lens, bent flatapole, transfer multipole: 7.9, 6.94, 5.9, 4 V, respectively). An optimized acceleration voltage (100–130 V) was then applied to the HCD cell to remove the detergent micelle from the protein ions. Backing pressure was maintained at $\sim 1.00 \times 10^{-3}$ mbar and data was analysed using Xcalibur 2.2 SP1.48.

The bound-lipid identification experiments were performed with a modified Synapt G2 mass spectrometer (Waters) equipped with a Z-spray source^{33,39}. The typical instrumental setting was source pressure (4.5–5.0 mbar), capillary voltage (1.2–1.5 kV) and cone voltage (100–200 V). An extraction voltage of 1–5 V was applied and 80–150 V was used as the collision voltage with argon as the collision gas

at a pressure of 0.2–0.3 MPa. To strip the detergent from protein ions in the source region, instrument values were optimized to capillary voltage (1.5 kV), cone voltage (200 V) and extraction voltage (3 V). A collision voltage ramp (from 20–100 V) was applied to dissociate protein-lipid complexes after quadrupole selection.

Identification of preferential PtdIns(4,5)P₂-binding sites on NTSR1. Unmodified NTSR1 and NTSR1 variants were pre-incubated at 1:1 molar ratio to produce a total protein concentration of 12 mM in protein buffer (10 mM HEPES pH 8, 150 mM NaCl, 0.01% (w/v) LMNG and 25% (v/v) glycerol). Detergent solubilised PI(4,5)P₂ was then added to the protein mixture at a final molar ratio of 1.25:1 lipid:receptor. The reaction mixture was incubated at 4 $^{\circ}\text{C}$ for 5 min and analysed by mass spectrometry after buffer exchanging to 200 mM ammonium acetate buffer containing the mix of detergents of DDM, LMNG and foscholine as described previously⁶.

The ratio of PtdIns(4,5)P₂ binding to the receptor was calculated by normalizing the intensity of the receptor in PtdIns(4,5)P₂-bound states to the unbound state using UniDec software. The results were evaluated by comparing the ratio of PtdIns(4,5)P₂ binding between mutants and the unmodified receptor and plotted as a bar chart using GraphPad Prism.

Mini-G_s and Nb6B9 coupling to β_1 AR. Effector coupling to β_1 AR was analysed using a modified Q-Exactive mass spectrometer after incubating purified β_1 AR with mini-G_s-Nb6B9 at 1:1.2 molar ratio at 4 $^{\circ}\text{C}$ in protein buffer (20 mM Tris-HCl, pH 7.4, 350 mM NaCl and 0.02% DDM). The relative percentage of effector coupling was quantified by UniDec software. A time course was performed with aliquots sampled after 2, 10, 30, and 60 min to monitor the formation of the mini-G_s-receptor complex. To investigate the effect of PtdIns(4,5)P₂ on coupling, β_1 AR was pre-incubated with detergent-solubilised PtdIns(4,5)P₂ at 1:1 molar ratio for 5 min at 4 $^{\circ}\text{C}$ to equilibrate before mixing with mini-G_s or Nb6B9 at 1.2 or 0.3 molar ratio to receptor, respectively. For the analogous PS binding experiment we pre-incubated β_1 AR with a threefold higher concentration of detergent solubilised PS than PtdIns(4,5)P₂ (PS: β_1 AR, 3:1 molar ratio) for 5 min at 4 $^{\circ}\text{C}$ to equilibrate before mixing with mini-G_s.

Modelling and simulation system setup. Simulations were performed using the GROMACS v.4.6.3 simulation package. Initial protein coordinates were obtained using PDB ID 4BUO (NTSR1) and PDB ID 2Y03 (β_1 AR), with missing atoms added using MODELLER⁴⁰. In the case of β_1 AR, a model was also constructed in which S68 in the thermostabilized structure 2Y03 was back-mutated to R68 to reconstruct available basic residues in the wild-type receptor using the mutagenesis tool implemented in PyMOL v.1.3r1. Side-chain ionisation states were modelled using pdb2gm⁴¹. The N and C termini were treated with neutral charge. Each protein structure was then energy minimized using the steepest descents algorithm implemented in GROMACS, before being converted to a coarse-grained representation using the MARTINI 2.2 force field⁴². The energy minimized coarse-grained structure was centred in a periodic simulation box with dimensions 11 \times 11 \times 12 nm³. POPC (1-palmitoyl-2-oleoyl-*sn*-glycero-3-phosphocholine) molecules were randomly placed around the protein and the system was solvated and neutralised to a concentration of 0.15 M NaCl. An initial 50 ns of coarse-grained simulation was applied to permit the self-assembly of a POPC lipid bilayer around the GPCR. POPC lipids were randomly exchanged⁴³ to create a mixed-species bilayer of specified composition (Extended Data Table 2). A cut-off distance of 2.5 nm was applied, with only molecules outside this distance being subject to exchange. The exchange protocol was conducted independently for each repeat simulation, such that different random initial configurations of lipids around the protein were generated for each simulation repeat. A summary of simulations performed is provided in Extended Data Table 2.

Simulation details. The MARTINI force field⁴² was used to describe all system components. An ELNEDYN network⁴⁴ was applied to the protein using a force constant of 500 kJ/mol/nm² and a cut off of 1.5 nm. Simulations were performed as an NPT ensemble, with temperature maintained at 310 K using a Berendsen thermostat⁴⁵ using a coupling constant of $\tau_t = 4$ ps, and semi-isotropic pressure controlled at 1 bar using a Berendsen barostat⁴⁵ with a coupling constant of $\tau_p = 4$ ps and a compressibility of 5×10^{-6} bar⁻¹. Electrostatics were modelled using the reaction field coulomb type⁴⁶, and smoothly shifted between 0 and 1.2 nm. Van der Waals interactions were treated using a shifting function between 0.9 and 1.2 nm. Covalent bonds were constrained to their equilibrium values using the LINCS algorithm⁴⁷. Equations of motion were integrated using the leap-frog algorithm, with a 20-fs time step. All simulations were run in the presence of conventional MARTINI water, and neutralised to a concentration of 0.15 M NaCl.

Analysis of simulation data was conducted using VMD⁴⁸, PyMOL, tools implemented in GROMACS⁴¹, and in-house protocols. Protein-lipid contact analysis employed a cut-off distance of 0.6 nm, based on radial distribution functions for coarse-grained lipid molecules⁴⁹.

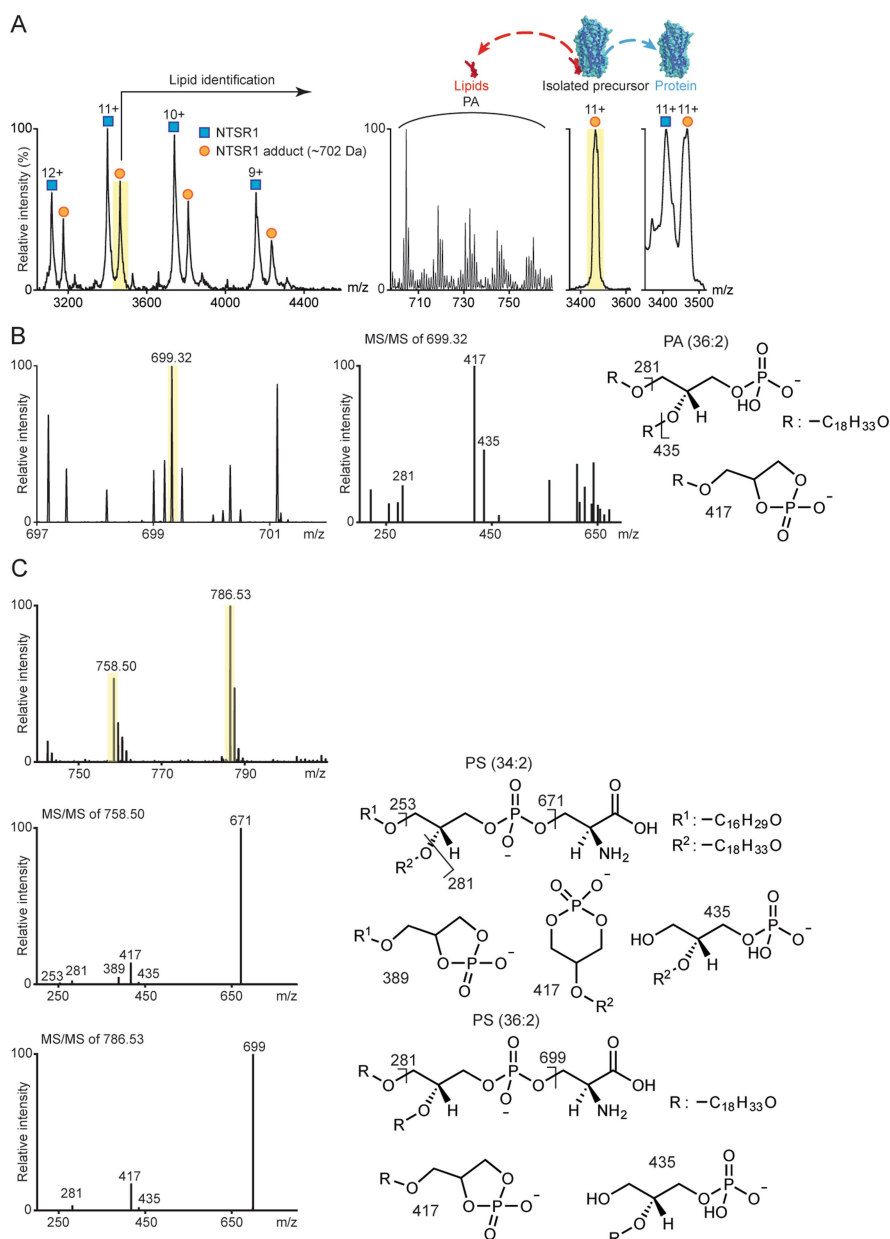
A_{2A}R-mini-G_s PMF calculations. PMFs for the interaction of mini-G_s with A_{2A}R in a lipid bilayer in the presence and absence of PtdIns(4,5)P₂ were calculated using the MARTINI force field⁵⁰. To obtain a PtdIns(4,5)P₂-bound A_{2A}R-mini-G_s complex,

we first ran ten coarse-grained molecular dynamics simulations on receptor embedded in an asymmetric complex membrane, each lasting 8 μ s (Extended Data Table 2). The r.m.s.d. to the crystal structure of A_{2A}R–mini-G_S complex (PDB ID 5G53) was calculated for the protein in these ten simulations, and the protein complex with the lowest r.m.s.d. was saved together with the membrane bilayer. The coarse grained mini-G_S was then docked back to the membrane-embedded receptor based on the A_{2A}R–mini-G_S crystal structure to generate the starting configuration of a steered molecular dynamics (SMD) simulation. In the SMD, the mini-G_S was pulled away from the receptor along the *z* axis (normal to the membrane plane) at a rate of 0.05 nm/ns using a force constant of 1000 kJ/mol/nm² while the receptor was restrained in place using a harmonic force of 1000 kJ/mol/nm². The distance between the centre of mass of the receptor and the mini-G_S was defined as the 1D reaction coordinate and the pulling process covered a distance of 3 nm. The initial configurations of the umbrella sampling were extracted from the SMD trajectory spacing 0.05 nm apart along the reaction coordinate. Fifty umbrella sampling windows were generated, and each was subjected to 1- μ s molecular dynamics simulation, in which a harmonic restraint of 1000 kJ/mol/nm² was imposed on the distance between the centre of mass of the receptor and the mini-G_S to maintain the separation of the two. The PMF was extracted from the umbrella sampling using the weighted histogram analysis method (WHAM) provided by the GROMACS *g_wham* tool⁵¹. A Bayesian bootstrap was used to estimate the statistical error of the energy profile. The PMF of the binding process in the absence of PtdIns(4,5)P₂ was calculated following the same protocol, with the only change made to the lipid composition of the membrane lower leaflet. PtdIns(4,5)P₂ was taken out from the membrane and instead the concentrations of POPC, 1,2-dioleoyl-*sn*-glycero-3-phosphocholine (DOPC), 1-palmitoyl-2-oleoyl-*sn*-glycero-3-phosphoethanolamine (POPE) and 1,2-dioleoyl-*sn*-glycero-3-phosphoethanolamine (DOPE) were increased by 2.5% to make up for the vacancy left by the absence of PtdIns(4,5)P₂.

Reporting summary. Further information on experimental design is available in the Nature Research Reporting Summary linked to this paper.

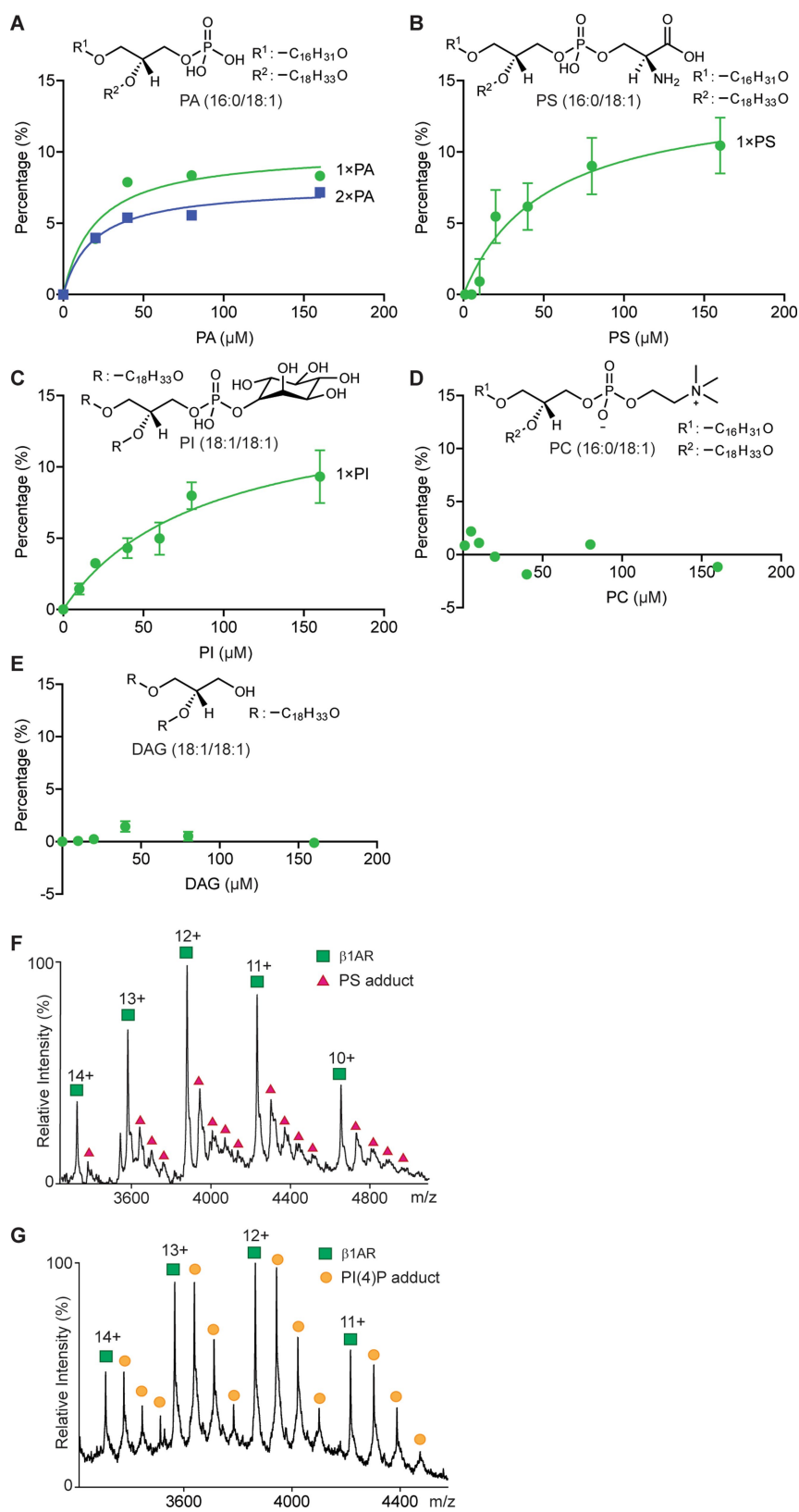
Data availability. All relevant data are available from corresponding authors on request.

24. Scott, D. J., Kummer, L., Eglöf, P., Bathgate, R. A. D. & Plückthun, A. Improving the apo-state detergent stability of NTS₁ with CHES for pharmacological and structural studies. *BBA-Biomembranes* **1838**, 2817–2824, (2014).
25. Carpenter, B. & Tate, C. G. Engineering a minimal G protein to facilitate crystallisation of G protein-coupled receptors in their active conformation. *Protein Eng. Des. Sel.* **29**, 583–594 (2016).
26. Warne, T. et al. Structure of a β_1 -adrenergic G-protein-coupled receptor. *Nature* **454**, 486–491 (2008).
27. Warne, T. et al. The structural basis for agonist and partial agonist action on a β_1 -adrenergic receptor. *Nature* **469**, 241–244 (2011).
28. Warne, T., Serrano-Vega, M. J., Tate, C. G. & Schertler, G. F. Development and crystallization of a minimal thermostabilised G protein-coupled receptor. *Protein Expr. Purif.* **65**, 204–213 (2009).
29. Warne, T., Chirnside, J. & Schertler, G. F. Expression and purification of truncated, non-glycosylated turkey beta-adrenergic receptors for crystallization. *Biochim. Biophys. Acta* **1610**, 133–140 (2003).
30. Carpenter, B. & Tate, C. G. Expression and Purification of Mini G Proteins from *Escherichia coli*. *Bio Protoc.* **7**, (2017).
31. Ring, A. M. et al. Adrenaline-activated structure of β_2 -adrenoceptor stabilized by an engineered nanobody. *Nature* **502**, 575–579 (2013).
32. Hillenbrand, M., Schori, C., Schoppe, J. & Plückthun, A. Comprehensive analysis of heterotrimeric G-protein complex diversity and their interactions with GPCRs in solution. *Proc. Natl Acad. Sci. USA* **112**, E1181–E1190 (2015).
33. Laganowsky, A., Reading, E., Hopper, J. T. S. & Robinson, C. V. Mass spectrometry of intact membrane protein complexes. *Nat. Protocols* **8**, 639–651 (2013).
34. Chen, P. S., Toribara, T. Y. & Warner, H. Microdetermination of phosphorus. *Anal. Chem.* **28**, 1756–1758 (1956).
35. Marty, M. T. et al. Bayesian deconvolution of mass and ion mobility spectra: from binary interactions to polydisperse ensembles. *Anal. Chem.* **87**, 4370–4376 (2015).
36. Bird, S. S., Marur, V. R., Sniatynski, M. J., Greenberg, H. K. & Kristal, B. S. Lipidomics profiling by high resolution LC–MS and HCD fragmentation: focus on characterization of mitochondrial cardiolipins and monolysocardiolipins. *Anal. Chem.* **83**, 940–949 (2011).
37. Bechara, C. et al. A subset of annular lipids is linked to the flippase activity of an ABC transporter. *Nat. Chem.* **7**, 255–262 (2015).
38. Eglöf, P., Deluigi, M., Heine, P., Balada, S. & Plückthun, A. A cleavable ligand column for the rapid isolation of large quantities of homogeneous and functional neurotensin receptor 1 variants from *E. coli*. *Protein Expr. Purif.* **108**, 106–114 (2015).
39. Sobott, F., Hernández, H., McCammon, M. G., Tito, M. A. & Robinson, C. V. A tandem mass spectrometer for improved transmission and analysis of large macromolecular assemblies. *Anal. Chem.* **74**, 1402–1407 (2002).
40. Sali, A. & Blundell, T. L. Comparative protein modelling by satisfaction of spatial restraints. *J. Mol. Biol.* **234**, 779–815 (1993).
41. Hess, B., Deluigi, C., van der Spoel, D. & Lindahl, E. GROMACS 4: algorithms for highly efficient, load-balanced, and scalable molecular simulation. *J. Chem. Theory Comput.* **4**, 435–447 (2008).
42. de Jong, D. H. et al. Improved parameters for the Martini coarse-grained protein force field. *J. Chem. Theory Comput.* **9**, 687–697 (2013).
43. Koldsø, H., Shorthouse, D., Hélie, J. & Sansom, M. S. P. Lipid clustering correlates with membrane curvature as revealed by molecular simulations of complex lipid bilayers. *PLOS Comput. Biol.* **10**, e1003911 (2014).
44. Periole, X., Cavalli, M., Marrink, S. J. & Ceruso, M. A. Combining an elastic network with a coarse-grained molecular force field: structure, dynamics, and intermolecular recognition. *J. Chem. Theory Comput.* **5**, 2531–2543 (2009).
45. Berendsen, H. J. C., Postma, J. P. M., van Gunsteren, W. F., DiNola, A. & Haak, J. R. Molecular dynamics with coupling to an external bath. *J. Chem. Phys.* **81**, 3684–3690 (1984).
46. Tironi, I. G., Sperb, R., Smith, P. E. & van Gunsteren, W. F. A generalized reaction field method for molecular dynamics simulations. *J. Chem. Phys.* **102**, 5451–5459 (1995).
47. Hess, B., Bekker, H., Berendsen, H. J. C. & Fraaije, J. G. E. M. LINCS: A linear constraint solver for molecular simulations. *J. Comput. Chem.* **18**, 1463–1472 (1997).
48. Humphrey, W., Dalke, A. & Schulten, K. VMD: visual molecular dynamics. *J. Mol. Graph.* **14**, 33–38 (1996).
49. Hedger, G., Sansom, M. S. P. & Koldsø, H. The juxtamembrane regions of human receptor tyrosine kinases exhibit conserved interaction sites with anionic lipids. *Sci. Rep.* **5**, 9198 (2015).
50. Hedger, G., Shorthouse, D., Koldsø, H. & Sansom, M. S. Free energy landscape of lipid interactions with regulatory binding sites on the transmembrane domain of the EGF receptor. *J. Phys. Chem. B* **120**, 8154–8163 (2016).
51. Hub, J. S., de Groot, B. L. & van der Spoel, D. *g_wham*—A free weighted histogram analysis implementation including robust error and autocorrelation estimates. *J. Chem. Theory Comput.* **6**, 3713–3720 (2010).
52. Notredame, C., Higgins, D. G. & Heringa, J. T-coffee: a novel method for fast and accurate multiple sequence alignment. *J. Mol. Biol.* **302**, 205–217 (2000).
53. Bond, C. S. & Schüttelkopf, A. W. ALiNE: a WYSIWYG protein-sequence alignment editor for publication-quality alignments. *Acta Crystallogr. D* **65**, 510–512 (2009).



Extended Data Fig. 1 | Identification of lipids bound to NTSR1 (HTGH4- Δ IC3B). **a**, Endogenous lipids bound to NTSR1 (HTGH4- Δ IC3B), isolated from *E. coli*, are identified as PA following m/z selection in the mass spectrometry quadrupole of the NTSR1:lipid 11+ charge state (highlighted yellow) and collisional activation to dissociate PA and its homologues (m/z , 700–760 Da). **b**, Lipidomics analysis of purified NTSR1 with three technical replicates

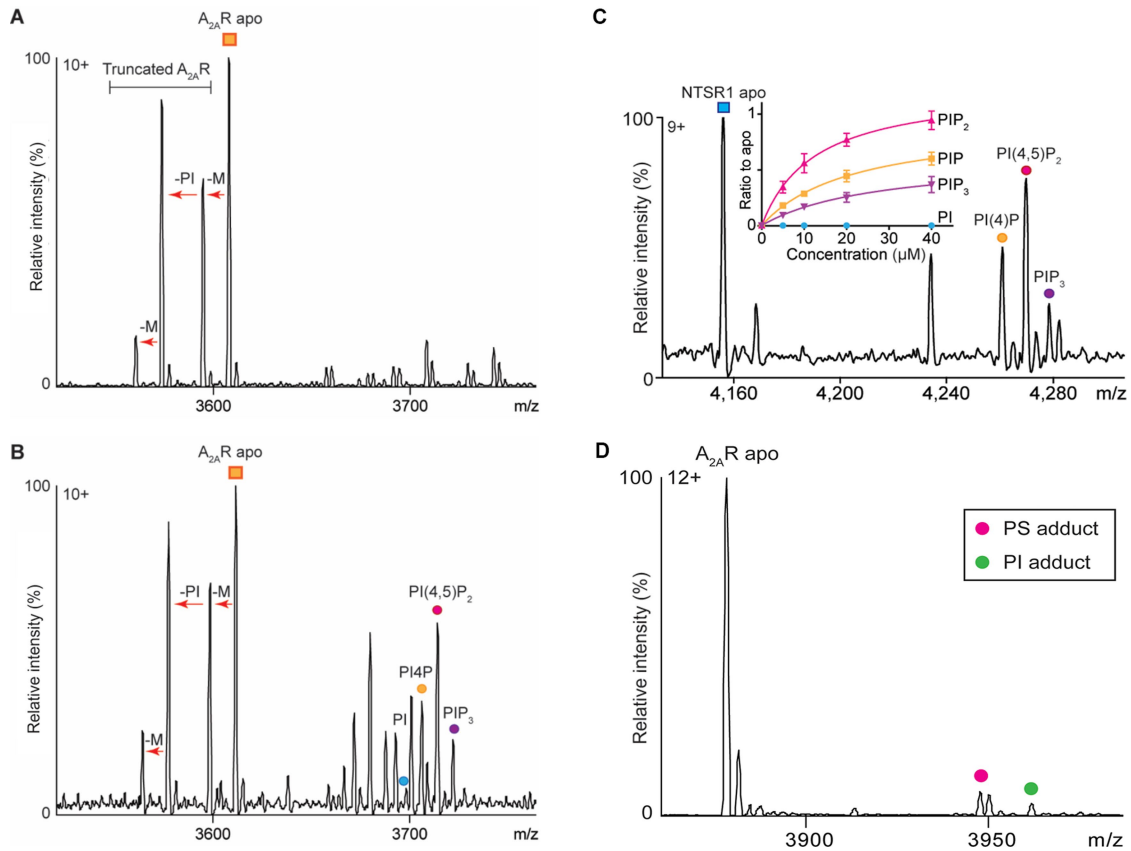
reveals peaks at low m/z . MS/MS spectra of the precursor ion (M-H-1) at m/z 699.32 highlighted yellow, leads to definitive fragment ions at m/z 281 and 417 consistent with the structure of PA (36:2). **c**, Analogous lipidomics analysis of purified β_1 AR from insect cells with three technical replicates. MS/MS spectra of the two [M-H-1] precursor ions (m/z 758.50 and 786.53) identified the lipids as PS (34:2) and PS (36:2) respectively with diagnostic fragments indicated.



Extended Data Fig. 2 | See next page for caption.

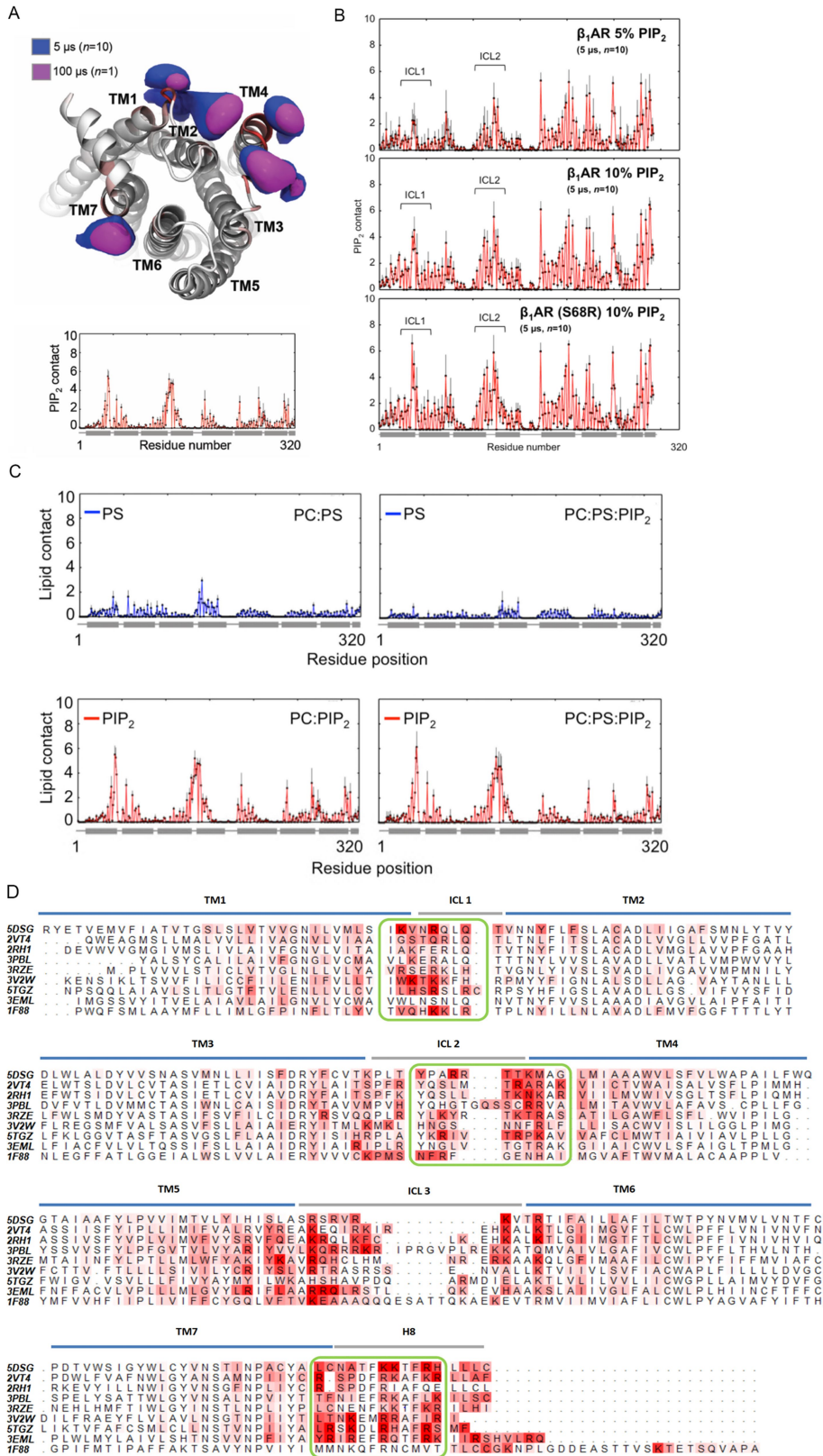
Extended Data Fig. 2 | Lipid-binding preference of NTSR1 and β_1 AR. **a–e**, The binding of NTSR1(HTGH4- Δ IC3B), measured by mass spectrometry ($n = 3$ independent experiments), to the phospholipids PA (**a**), PS (**b**), PI (**c**), PC (**d**) and DAG (**e**). The measurements were performed at different lipid concentrations (0 to 160 μ M) and the percentages of individual lipid-binding peaks (sum of apo protein and all lipid adducts obtained in the region of the mass spectrum under study) were plotted against lipid concentrations in solution. The lipid-binding curves were deduced from fitting to one-site total binding. Values of s.d. were calculated from three independent replicate experiments at each concentration. The results show that NTSR1 interacts preferentially

with anionic phospholipids (PA and PS), as no binding was observed for neutral (DAG) and zwitterionic (PC) lipids. **f, g**, Exogenous POPS (**f**) and PtdIns(4)P (**g**) were added to β_1 AR at different final concentrations (10 μ M is shown here). Spectra were recorded for a range of lipid concentrations from 0 to 80 μ M for PS and 0 to 20 μ M for PtdIns(4)P. Peak intensities of the individual PtdIns(4)P-bound species were measured and plotted against lipid concentration to yield a relative affinity for one PtdIns(4)P binding (1 \times), two PtdIns(4)P molecules binding (2 \times) or three PtdIns(4)P molecules binding (3 \times); only the first PtdIns(4)P molecule binds with high affinity (see Fig. 1a). Data are mean \pm s.d. from three independent experiments.



Extended Data Fig. 3 | Investigation of the phospholipid preferences of $A_{2A}R$ and NTSR1. **a**, A representative mass spectrum of purified $A_{2A}R$ from three independent experiments revealed truncations of the N-terminal sequence (MPIM). The arrows between species indicate the mass differences corresponding to truncated amino acids (M, PI and M). **b**, A competitive binding assay ($n = 3$ independent experiments) in which $A_{2A}R$ was incubated with a mixture of lipids (PI, PtdIns(4)P, PI(4,5) P_2 , and PtdIns(3,4,5) P_3) before mass spectrometry, indicated that PtdIns(4,5) P_2 binds with a higher affinity than the other phospholipids to $A_{2A}R$. **c**, The analogous competitive binding assay, in which NTSR1 was incubated with

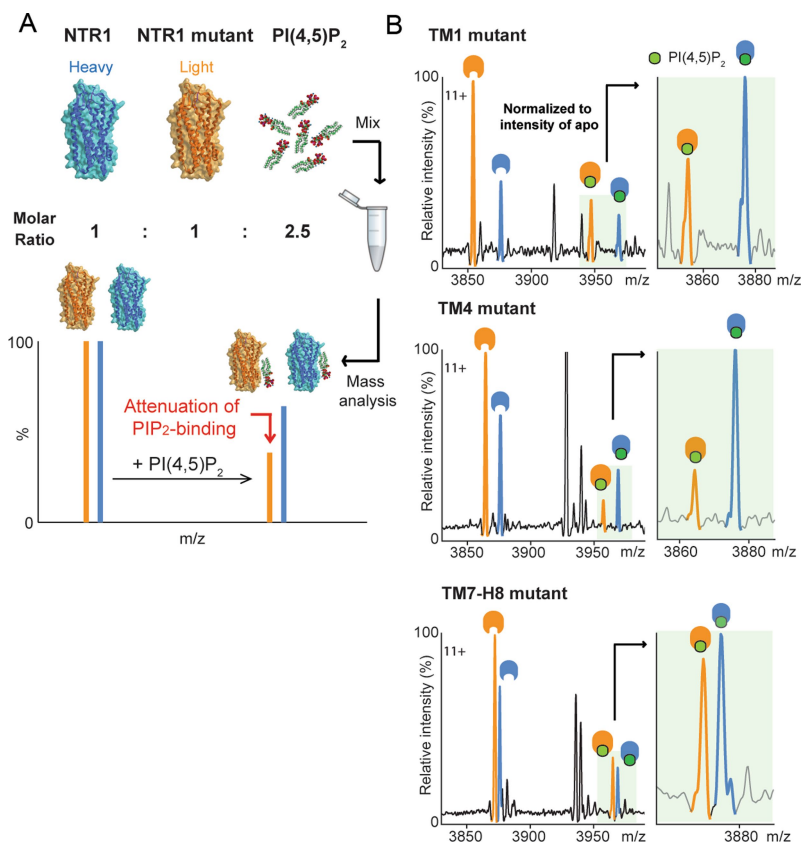
a mixture of lipids (PI, PtdIns(4)P, PI(4,5) P_2 and PtdIns(3,4,5) P_3) before mass spectrometry. Ratio to apo is plotted as a function of concentration and defined as the ratio of the intensity corresponding to individual PI phosphate adducts to the receptor in the apo state (inset). The same data analysis methods are used for Fig. 1b. PtdIns(4,5) P_2 binds with a higher affinity than the other phospholipids to $A_{2A}R$. Data are shown as mean \pm s.d. from three independent replicates. **d**, A representative mass spectrum of $A_{2A}R$ ($n = 3$ independent experiments) used for preparation of the G-protein complex reveals lower abundance of PS and PI adducts prior to coupling to G proteins.



Extended Data Fig. 4 | See next page for caption.

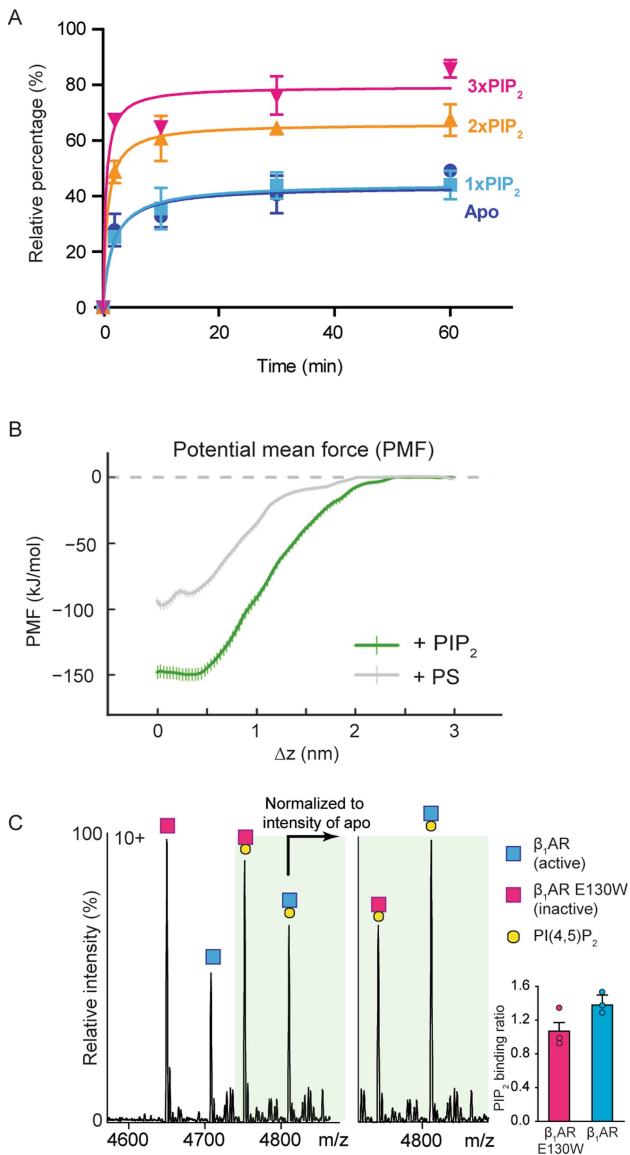
Extended Data Fig. 4 | NTSR1–PtdIns(4,5)P₂ and β_1 AR–PtdIns(4,5)P₂ interactions within CGMD simulations, and comparison of PtdIns(4,5)P₂ contacts among different GPCRs. **a**, Volumetric density surfaces showing the average spatial occupancy of PtdIns(4,5)P₂ lipids around a crystal structure of NTSR1 (TM86V- Δ IC3B) (PDB: 4BUO), which shares a greater sequence identity to the wild-type receptor (91%) than NTSR1 (HTGH4- Δ IC3B) (86%), contoured to show the major PtdIns(4,5)P₂-interaction sites. Density surfaces were calculated over 5 μ s of CGMD (blue surface, $n = 10$ independent experiments), and 100 μ s of CGMD (magenta, $n = 1$ experiment). The cytoplasmic side of NTSR1 structure is coloured from white (low PtdIns(4,5)P₂ interaction) to red (high PtdIns(4,5)P₂ interaction). Extending a simulation to 100 μ s revealed no overall change in the patterns of PtdIns(4,5)P₂ interaction. Less specific, and hence more dynamic, interaction was seen for the acyl chain moieties of PtdIns(4,5)P₂, which yielded more diffuse probability densities. **b**, β_1 AR–PtdIns(4,5)P₂ interactions within CGMD simulations. Contact patterns are shown for simulations containing 5% PtdIns(4,5)P₂ in the lipid bilayer and thermostable β_1 AR (PDB: 2Y03, top), 10% PtdIns(4,5)P₂ and thermostable β_1 AR (middle), and 10% PtdIns(4,5)P₂ and β_1 AR(S68R) construct (bottom). In each case PtdIns(4,5)P₂ contacts were calculated over 5 μ s of CGMD ($n = 10$ independent experiments; error bars, s.d.), with each repeat simulation initiated from different random system

configurations. **c**, PS and PtdIns(4,5)P₂ contacts with NTSR1 as a function of residue position, for PC:PS membranes (top left), PC:PS:PtdIns(4,5)P₂ membranes (top right), PC:PtdIns(4,5)P₂ membrane (bottom left) and PC:PS:PtdIns(4,5)P₂ (bottom right). The position of helices is denoted by horizontal grey bars. Lipid contact is calculated as the mean number of contacts between each residue and a given lipid species per frame, using a 6 Å distance cut-off. $n = 3$; error bars, s.d. **d**, PtdIns(4,5)P₂ contacts seen in CGMD simulations for nine class A GPCRs: histamine H1 receptor, PDB 3RZE; β_1 adrenergic receptor, 2VT4; β_2 adrenergic receptor, 2RH1; CB1 cannabinoid receptor, 5TGZ; M4 muscarinic acetylcholine receptor, 5DSG; adenosine A_{2A} receptor, 3EML; dopamine D3 receptor, 3PBL; sphingosine 1-phosphate receptor, 3V2W; rhodopsin, 1F88. GPCR sequences are shown, with TM helices, intracellular loops (ICL) and H8 helices indicated by horizontal bars, and with amino acids coloured according to the mean number of contacts per simulation frame with the PtdIns(4,5)P₂ molecules. Green boxes correspond to the high frequency of PtdIns(4,5)P₂ interactions discussed in the main text for the TM1, TM4, and TM7/H8 motifs of NTSR1. Contacts were computed over 1 μ s CGMD simulations ($n = 3$ independent experiments) for each GPCR, using a 6 Å cut-off. Sequences were aligned using T-Coffee⁵² and mapping of protein–lipid contact data onto the sequence alignment used ALINE⁵³.

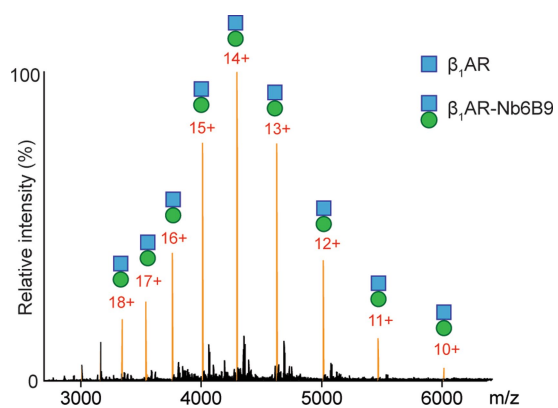


Extended Data Fig. 5 | Site-directed mutagenesis attenuates PtdIns(4,5)P₂ binding to NSTR1. **a**, Schematic representation of the experimental protocol designed to combine mass spectrometry with mutagenesis to produce mutants of lower molecular mass than wild type, which, when incubated with PtdIns(4,5)P₂, yield a direct readout of the effect of mutations in specific regions. **b**, PtdIns(4,5)P₂ binding of NTSR1 mutants on residues that exhibit the highest frequency of PtdIns(4,5)P₂ interaction in molecular dynamics simulation. Mutation of NTSR1 (HTGH4- Δ IC3B) residues on TM1 (R46G, K47G and K48G (R43G, K44G and K45G in NTSR1(TM86- Δ IC3B); R91G, K92G, K93G in wild type)), TM4

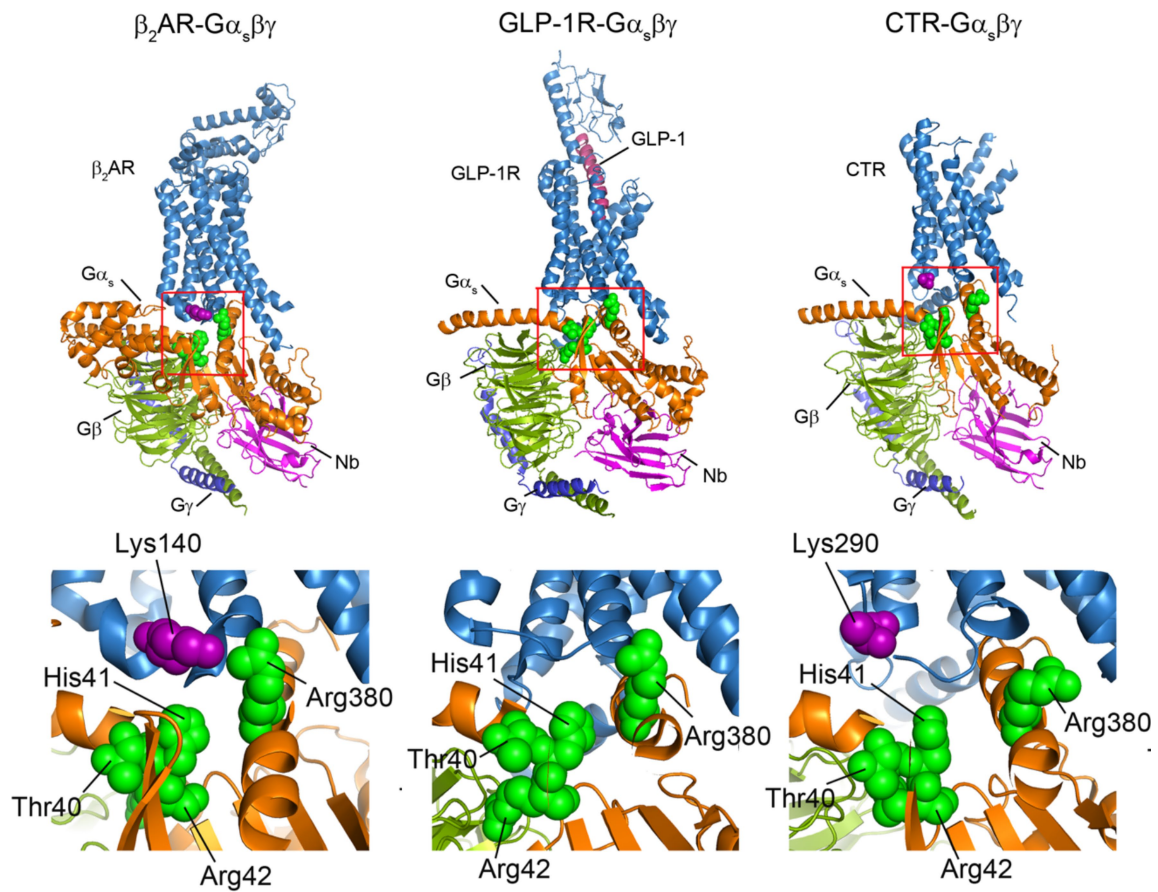
(R138I, R140T, K142L and K143L (R135I, R137T, K139L and K140L in NTSR1(TM86- Δ IC3B); R183I, R185T, K187L and K188L in wild type)) and TM7-H8 (R316N (R311N in NTSR1(TM86- Δ IC3B); R377N in wild type)) attenuate PtdIns(4,5)P₂ binding, and indicate that the TM4 interface is a preferential binding site over TM1 and TM7-H8 interfaces. Selection of residues for mutations was guided by molecular dynamics (Extended Data Fig. 4) and previous studies in which binding of a fluorescently labelled agonist, BODIPY neurotensin, to NTSR1, was screened and used to monitor efficient production, insertion, and folding¹⁰.



Extended Data Fig. 6 | PtdIns(4,5)P₂ binds preferentially to β₁AR in an active state and stabilizes β₁AR coupled to mini-G_s and A₂AR-mini-G_s complex. **a**, A time-course experiment was performed to monitor the formation of active β₁AR–mini-G_s complex. The coupling efficiency (percentage) was calculated from the relative intensity of peaks assigned to β₁AR–mini-G_s coupling in the appropriate lipid-bound state. The plot indicates that mini-G_s coupling is enhanced by PtdIns(4,5)P₂ when more than two lipid molecules are bound to the receptor. Error bars represent s.d. from at least three independent experiments. **b**, Plot of PMF for the interaction of mini-G_s with A₂AR in the presence of PtdIns(4,5)P₂ (green) or PS (grey). The PMF is calculated along a reaction coordinate (Δz) corresponding to the centre–centre separation of the mini-G_s and receptor proteins along the z axis (normal to the bilayer plane). The interaction of mini-G_s with the A₂AR is stabilized in the presence of PtdIns(4,5)P₂ by 50 ± 10 kJ mol⁻¹ relative to PS. Error bars (which are <10 kJ mol⁻¹) are from bootstrap sampling of the PMFs and therefore represent the ‘statistical’ errors in estimating the well depth from a given set of simulations and PMF calculation (*n* = 3 independent experiments). We therefore estimate a minimum error of ≤10 kJ mol⁻¹. **c**, Mass spectra were recorded for a 1:1 equimolar mix of an inactive unliganded β₁AR variant, E130W, and its unmodified active counterpart (co-purified with the agonist isoprenaline) in the presence of PI(4,5)P₂. Lipid binding occurred on both receptors, but following normalization to account for differences in ionization efficiency, a clear preference for PtdIns(4,5)P₂ binding to the active receptor was observed. Bars represent mean ± s.d.



Extended Data Fig. 7 | Detection of nanobody coupling to β_1 AR. Peaks in the mass spectrum assigned to Nb6B9 binding to β_1 AR to form an equimolar β_1 AR-Nb6B9 complex are highlighted in orange, and demonstrate complete complex formation, implying that nanobody has a higher affinity than mini-G_s for β_1 AR. $n = 3$ independent experiments.



Extended Data Fig. 8 | Structural comparison of class A and class B GPCRs in complex with trimeric $G\alpha\beta\gamma$ complexes. The PtdIns(4,5) P_2 contacts of the $G\alpha_s$ subunit observed in molecular dynamics simulations (green spheres) are highlighted on the structures of trimeric G-protein interactions with β_2 AR (PDB: 3SN6), the glucagon-like peptide-1 receptor (GLP-1) (PDB: 5VAI) and the calcitonin receptor (CTR) (PDB: 5UZ7).

Basic residues on the interface adjacent to the cytoplasmic end of TM4 are highlighted as purple spheres. Lower panels show an expanded view, highlighting the conserved pattern of PtdIns(4,5) P_2 bridging in class A GPCRs (β_2 AR and A_{2A} R (Fig. 3e)), both of which have basic residues on TM4 (Lys140 and Arg107/111) that are not present in the class B GPCRs GLP-1R and CTR.

Extended Data Table 1 | Lipidomics analysis of purified β_1 AR

Mass (Da)	Lipid ID
824.61	PC (36:0)
716.52	PE (34:1)
742.54	PE (36:2)
714.51	PE (34:2)
772.59	PE (38:1)
752.57	PE (37:4)
793.57	PG (38:6)
807.50	PI (32:1)
833.52	PI (34:2)
865.58	PI (36:0)
835.53	PI (34:1)
863.57	PI (36:1)
861.55	PI (36:2)
891.60	PI (38:1)
758.50	PS (34:2)
760.51	PS (34:1)
786.53	PS (36:2)
1019.60	PIP (42:5)
1343.90	CL (64:4)
1371.93	CL (66:4)
1399.96	CL (68:4)

Extended Data Table 2 | Simulations run

Name	Length	Bilayer Composition
NTSR1	10 x 5 μ s	POPC(95%):PIP ₂ (5%)
NTSR1	3 x 5 μ s	POPC(95%):PS(5%)
NTSR1	10 x 5 μ s	POPC(95%):PS(5%):PIP ₂ (5%)
NTSR1 extended	1 x 100 μ s	POPC(95%):PIP ₂ (5%)
β_1 AR (5%)	10 x 5 μ s	POPC(95%):PIP ₂ (5%)
β_1 AR (10%)	10 x 5 μ s	POPC(90%):PIP ₂ (10%)
β_1 AR (S68R, 10%)	10 x 5 μ s	POPC(90%):PIP ₂ (10%)
A _{2A} R-mini-Gs	10 x 8 μ s	POPC(95%):PIP ₂ (5%)

Lipids were symmetrically distributed between leaflets.

Reporting Summary

Nature Research wishes to improve the reproducibility of the work that we publish. This form provides structure for consistency and transparency in reporting. For further information on Nature Research policies, see [Authors & Referees](#) and the [Editorial Policy Checklist](#).

Statistical parameters

When statistical analyses are reported, confirm that the following items are present in the relevant location (e.g. figure legend, table legend, main text, or Methods section).

n/a Confirmed

- The exact sample size (n) for each experimental group/condition, given as a discrete number and unit of measurement
- An indication of whether measurements were taken from distinct samples or whether the same sample was measured repeatedly
- The statistical test(s) used AND whether they are one- or two-sided
Only common tests should be described solely by name; describe more complex techniques in the Methods section.
- A description of all covariates tested
- A description of any assumptions or corrections, such as tests of normality and adjustment for multiple comparisons
- A full description of the statistics including central tendency (e.g. means) or other basic estimates (e.g. regression coefficient) AND variation (e.g. standard deviation) or associated estimates of uncertainty (e.g. confidence intervals)
- For null hypothesis testing, the test statistic (e.g. F , t , r) with confidence intervals, effect sizes, degrees of freedom and P value noted
Give P values as exact values whenever suitable.
- For Bayesian analysis, information on the choice of priors and Markov chain Monte Carlo settings
- For hierarchical and complex designs, identification of the appropriate level for tests and full reporting of outcomes
- Estimates of effect sizes (e.g. Cohen's d , Pearson's r), indicating how they were calculated
- Clearly defined error bars
State explicitly what error bars represent (e.g. SD, SE, CI)

Our web collection on [statistics for biologists](#) may be useful.

Software and code

Policy information about [availability of computer code](#)

Data collection

We have used, MassLynx V4.1 and Xcalibur 2.2 mass spectra acquisition. GROMACS43 was used for performing molecular dynamics simulation.

Data analysis

UniDec was used mass spectra analysis.VMD50, PyMOL V1.3r1 and tools implemented in GROMACS43 were used for analysis of simulation data. All other data were plotted used Prism. These software are ready available.

For manuscripts utilizing custom algorithms or software that are central to the research but not yet described in published literature, software must be made available to editors/reviewers upon request. We strongly encourage code deposition in a community repository (e.g. GitHub). See the Nature Research [guidelines for submitting code & software](#) for further information.

Data

Policy information about [availability of data](#)

All manuscripts must include a [data availability statement](#). This statement should provide the following information, where applicable:

- Accession codes, unique identifiers, or web links for publicly available datasets
- A list of figures that have associated raw data
- A description of any restrictions on data availability

The data that support the findings of this study are available from the corresponding author upon reasonable request.

Field-specific reporting

Please select the best fit for your research. If you are not sure, read the appropriate sections before making your selection.

Life sciences Behavioural & social sciences Ecological, evolutionary & environmental sciences

For a reference copy of the document with all sections, see [nature.com/authors/policies/ReportingSummary-flat.pdf](https://www.nature.com/authors/policies/ReportingSummary-flat.pdf)

Life sciences study design

All studies must disclose on these points even when the disclosure is negative.

Sample size	No sample size calculations were performed. All proteins were selected based on underlining biology and availability
Data exclusions	No data were excluded from the analysis
Replication	All measurements were done in triplicate and all attempts at replication were successful and presented
Randomization	There was no allocation into experimental groups involved
Blinding	Blinding is not relevant to this study, no in vivo studies were used

Reporting for specific materials, systems and methods

Materials & experimental systems

n/a	Included in the study
<input type="checkbox"/>	<input checked="" type="checkbox"/> Unique biological materials
<input type="checkbox"/>	<input checked="" type="checkbox"/> Antibodies
<input type="checkbox"/>	<input checked="" type="checkbox"/> Eukaryotic cell lines
<input checked="" type="checkbox"/>	<input type="checkbox"/> Palaeontology
<input checked="" type="checkbox"/>	<input type="checkbox"/> Animals and other organisms
<input checked="" type="checkbox"/>	<input type="checkbox"/> Human research participants

Methods

n/a	Included in the study
<input checked="" type="checkbox"/>	<input type="checkbox"/> ChIP-seq
<input checked="" type="checkbox"/>	<input type="checkbox"/> Flow cytometry
<input checked="" type="checkbox"/>	<input type="checkbox"/> MRI-based neuroimaging

Unique biological materials

Policy information about [availability of materials](#)

Obtaining unique materials All unique materials are readily available from authors, with a reasonable request

Antibodies

Antibodies used	Nanobodies were expressed in E.coli strain BL21(DE3)RIL (Agilent Technologies), using synthetic genes
Validation	The validation of the nanobodies is shown by Ring 2013, Rasmussen 2011

Eukaryotic cell lines

Policy information about [cell lines](#)

Cell line source(s)	Sf9 and Tni (High 5™) cells were obtained from Invitrogen
Authentication	The cell line was authenticated by the supplier. None of the cell line used have been authenticated by the authors.
Mycoplasma contamination	Cell lines tested negative for mycoplasma contamination
Commonly misidentified lines (See ICLAC register)	No commonly misidentified cell lines were used